

## THE CENTRAL MASS DISTRIBUTION IN DWARF AND LOW SURFACE BRIGHTNESS GALAXIES

R. A. SWATERS

Department of Physics and Astronomy, Johns Hopkins University, 3400 N. Charles Str., Baltimore, MD 21218, Space Telescope Science Institute, 3700 San Martin Dr., Baltimore, MD 21218, and Department of Terrestrial Magnetism, Carnegie Institution of Washington, 5241 Broad Branch Rd NW, Washington, DC 20015

B. F. MADORE

Observatories of the Carnegie Institution of Washington and NASA/IPAC Extragalactic Database, California Institute of Technology, Pasadena CA 91125, USA

FRANK C. VAN DEN BOSCH

Max Planck Institut für Astrophysik, Karl Schwarzschild Str. 1, Postfach 1317, 85741 Garching, Germany

AND

M. BALCELLS

Instituto de Astrofísica de Canarias, E-38200 La Laguna, Tenerife, Spain

*The Astrophysical Journal, accepted Oct 2, 2002*

### ABSTRACT

We present high-resolution H $\alpha$  rotation curves for a sample of 15 dwarf and low surface brightness galaxies. From these, we derive limits on the slopes of the central mass distributions, using both a direct inversion of the rotation curves as well as detailed mass models. Assuming the density distributions of dark matter halos follow a power-law at small radii,  $\rho(r) \propto r^{-\alpha}$ , we find inner slopes in the range  $0 \lesssim \alpha \lesssim 1$  for most galaxies. Thus, even with the relatively high spatial resolution of the H $\alpha$  rotation curves presented here the inner slopes are poorly constrained. In general, halos with constant density cores ( $\alpha = 0$ ) provide somewhat better fits, but the majority of our galaxies ( $\sim 75$  percent) are also consistent with  $\alpha = 1$ , as long as the *R*-band stellar mass-to-light ratios are smaller than about 2. Halos with  $\alpha = 1.5$ , however, are ruled out in virtually every case. In order to investigate the robustness of these results we discuss and model several possible causes of systematic errors including non-circular motions, galaxy inclination, slit width, seeing, and slit alignment errors. Taking the associated uncertainties into account, we conclude that even for the  $\sim 25$  percent of the cases where  $\alpha = 1$  seems inconsistent with the rotation curves, we cannot rule out cusp slopes this steep. Inclusion of literature samples similar to the one presented here leads to the same conclusion when the possibility of systematic errors is taken into account. In the ongoing debate on whether the rotation curves of dwarf and low surface brightness galaxies are consistent with predictions for a cold dark matter universe, we argue that our sample and the literature samples discussed in this paper provide insufficient evidence to rule out halos with  $\alpha = 1$ . At the same time, we note that none of the galaxies in these samples require halos with steep cusps, as most are equally well or better explained by halos with constant density cores.

*Subject headings:* galaxies: dwarfs — galaxies: halos — galaxies: kinematics and dynamics

### 1. INTRODUCTION

Cosmological simulations based on different properties of dark matter make distinct predictions for the properties of the dark matter halos. The inner slope  $\alpha$  of the central power-law density distribution  $\rho(r) \propto r^{-\alpha}$  is particularly sensitive to the adopted properties of dark matter. If, for example, the dark matter is assumed to be cold and collisionless (CDM), the equilibrium density profiles of the dark halos will have steep inner slopes. Early simulations found  $\alpha = 1$  (Dubinski & Carlberg 1991, Navarro, Frenk, & White 1996, 1997), but later simulations found steeper slopes with  $\alpha = 1.5$  (Fukushige & Makino 1997; Moore et al. 1998, 1999; Davé et al. 2001; Klypin et al. 2001). A recent comprehensive study of the effects of numerical parameters by Power et al. (2002) places an upper limit on the inner slope of  $\alpha = 1.2$ , and suggests that the disagreement in the literature on the value of  $\alpha$  is mainly due to resolution issues in the numerical simulations. If the dark matter is assumed to be warm (WDM), cores with  $\alpha \sim 1$  are found (Colín, Avila-Reese, & Valenzuela 2000; Knebe et al. 2002), and shallower slopes are found for self-interacting dark matter (SIDM, Davé et al. 2001). Because of these differences in inner slopes it may

be possible to obtain limits on the nature of dark matter from the observed rotation curves of disk galaxies.

Unfortunately, it has proved remarkably hard to establish the inner slope of the dark matter distribution observationally. The inner slope is usually constrained by fitting the observed rotation curves with mass models that contain both the dark and luminous components. However, because the mass-to-light ratio (M/L) of the stellar disk is not known, a large degeneracy exists in the mass modeling (e.g., van Albada et al. 1985; Lake & Feinswoog 1989). As a result, the observed rotation curves can often be explained by a wide range in mass models, ranging from mass models in which the stellar disk dominates in the inner parts and where the halo has a shallow inner profile (e.g., Begeman 1987, 1989), to ones in which the stellar disk is less important and the mass distribution is dominated by a centrally concentrated halo (e.g., Verheijen 1997; Navarro 1998).

This degeneracy can be partially avoided by studying dwarf and low surface brightness (LSB) galaxies. Even though the central parts of the observed rotation curves can in principle be explained by scaling up the contribution of the stellar disks (Swaters 1999, hereafter S99; Swaters, Madore, &

TABLE 1  
GLOBAL PROPERTIES

Name	R.A. (J2000)			Dec. (J2000)			$M_R$	$h$	$\mu_R$	$D$	$v_{\text{sys}}$	$i$	$\phi$	notes
(1)	(2)		(3)				(mag)	(kpc)	(mag $h^{-2}$ )	(Mpc)	(km $s^{-1}$ )	( $^{\circ}$ )	( $^{\circ}$ )	(11)
							(4)	(5)	(6)	(7)	(8)	(9)	(10)	
UGC 731	1	10	43.6	49	36	4	-16.6	1.65	23.0	8.0	638	57	77	barred
UGC 2259	2	47	55.6	37	32	17	-17.8 <sup>a</sup>	1.29 <sup>a</sup>	21.2 <sup>a</sup>	9.8	574	41	160	
UGC 4325	8	19	19.7	50	0	32	-18.1	1.63	21.6	10.1	527	41	53	
UGC 4499	8	37	41.4	51	39	9	-17.8	1.49	21.5	13.0	693	50	140	barred
UGC 5721	10	32	17.3	27	40	8	-16.6	0.45	20.2	6.7	535	61	96	
UGC 8490	13	29	36.4	58	25	12	-17.3	0.66	20.5	4.9	208	50	170	
UGC 11557	20	24	0.7	60	11	41	-19.7	3.10	21.0	23.8	1388	30	94	
UGC 11707	21	14	31.7	26	44	5	-18.6	4.30	23.1	15.9	904	68	57	
UGC 11861	21	56	24.2	73	15	39	-20.8	6.06	21.4	25.1	1481	50	39	barred
UGC 12732	23	40	39.8	26	14	11	-18.0	2.21	22.4	13.2	749	39	14	
F 563-V2	8	53	3.7	18	26	9	-19.0 <sup>b</sup>	2.10 <sup>b</sup>	21.3 <sup>b</sup>	61	4310	29	148	barred
F 568-1	10	26	6.3	22	26	1	-18.9	4.41	22.7	85	6524	26	13	
F 568-3	10	27	20.3	22	14	22	-19.2	4.48	22.4	77	5911	40	169	barred
F 568-V1	10	45	2.1	22	3	16	-18.7	3.96	22.7	80	5769	40	136	
F 574-1	12	38	7.1	22	18	50	-19.2	4.24	22.2	96	6889	65	90	

Notes — (1) the name of the galaxy, (2) and (3) the coordinates, (4) the absolute  $R$ -band magnitude, (5) the scale length, (6) the  $R$ -band extrapolated central disk surface brightness, (7) the adopted distance, based on a Hubble constant of  $75 \text{ km s}^{-1} \text{Mpc}^{-1}$  or on a secondary distance indicator (see Swaters & Balcells 2002) (8) the HI heliocentric systemic velocity, (9) the inclination, (10) the position angle of the major axis, and (11) notes on galaxy morphology, as judged from deep CCD imaging presented in Swaters & Balcells (2002) and de Blok et al. (1995). The data for UGC 2259 have been taken from Carignan, Sancisi, & van Albada 1988, the data for the remaining UGC galaxies comes from Swaters 1999, the data for the LSB galaxies comes from McGaugh & Bothun 1994 and de Blok et al. 1995, 1996.

<sup>a</sup> Converted from  $I$ -band observations assuming  $R-I=0.5$ . <sup>b</sup> Converted from  $B$ -band observations assuming  $B-R=0.8$ .

Trewhella 2000, hereafter SMT), the inferred stellar M/Ls are much higher than expected from population synthesis modeling (e.g., Worthey 1994; Bell & de Jong 2001). For reasonable stellar M/Ls, these galaxies are then dominated by dark matter at all radii, making dwarf and LSB galaxies very suitable for studies of the properties of dark matter.

Consequently, the rotation curves of these galaxies have received a great deal of attention. Early studies found that these galaxies have slowly rising inner rotation curves and that their halos can be well described by pseudo-isothermal spheres with constant density cores (e.g., Carignan & Beaulieu 1989; Côté, Carignan, & Sancisi 1991; Broeils 1992a, 1992b; Côté 1995; de Blok & McGaugh 1997). Because of their shallow slopes, these rotation curves were stated to be inconsistent with the steep halos predicted by cold dark matter (Moore 1994; Flores & Primack 1994; Navarro et al. 1996; McGaugh & de Blok 1998). Recent studies raised the concern that some of these HI rotation curves may have been affected by beam smearing due to the poor angular resolution of the HI observations, and found that the rotation curves of dwarf and LSB galaxies rise more steeply when beam smearing is taken into account (S99; Blais-Ouellette et al. 1999; SMT). Fitting beam-smeared mass models to the HI rotation curves indicated that dwarf and LSB galaxies are consistent with a wide range of dark matter properties, ranging from constant density cores to steep cusps with  $\alpha = 1$ . However, slopes with  $\alpha = 1.5$  appear difficult to reconcile with the observations (van den Bosch et al. 2000; Swaters 2001a; van den Bosch & Swaters 2001, hereafter vdBS).

HI observations, however, with typical resolutions of  $15''$ , may not be best suited to determine the inner rotation curve slopes. The large range in mass models that are consistent with the observations might simply be a reflection of the systematic effects caused by the HI observations. High angular resolution observations, for example based on  $\text{H}\alpha$  long slit or Fabry-Perot

spectroscopy seem more suited to measure the inner slopes. Yet even among studies based on such high angular resolution observations a controversy remains. On the one hand, there are studies that find that dwarf and LSB galaxies may have steep inner slopes (Swaters 2001b; Pickering et al., in preparation), and on the other hand there are several studies that find that these galaxies are not consistent with steep inner slopes (Borriello & Salucci 2001; Dalcanton & Bernstein 2000; Blais-Ouellette, Amram, & Carignan 2001; de Blok et al. 2001a, hereafter dBMBR; de Blok et al. 2001b, hereafter dBM; de Blok & Bosma 2002, hereafter dBB; Marchesini et al. 2002).

This paper presents new  $\text{H}\alpha$  long slit spectroscopy for a sample of 15 dwarf and LSB galaxies, and directly addresses the halo cusp slope controversy outlined above. We measure the inner slopes of the mass distributions, and determine the range of mass models consistent with the observations, taking account of possible systematic effects. In Section 2 we describe the sample and the observations. Section 3 covers the derivation of the rotation curves. In Section 4 we describe the mass models fitted to the rotation curves, and in Section 5 we present the results from the mass modeling. In Section 6 the systematic effects that may have affected the derived rotation curves and inner slopes are discussed, and in Section 7 we model how these systematic effects affect the data. In Section 8 we discuss our results, and we compare our results to those in the literature, and to predictions made by cosmological simulations. In Section 9 we present our conclusions.

## 2. SAMPLE AND OBSERVATIONS

The dwarf galaxies presented here were taken from the sample of S99, and the LSB galaxies were taken from the sample of de Blok, McGaugh, & van der Hulst (1996). The UGC galaxies in our sample are dwarf galaxies, the remaining five galaxies are LSB galaxies. We note that the properties of dwarf and LSB

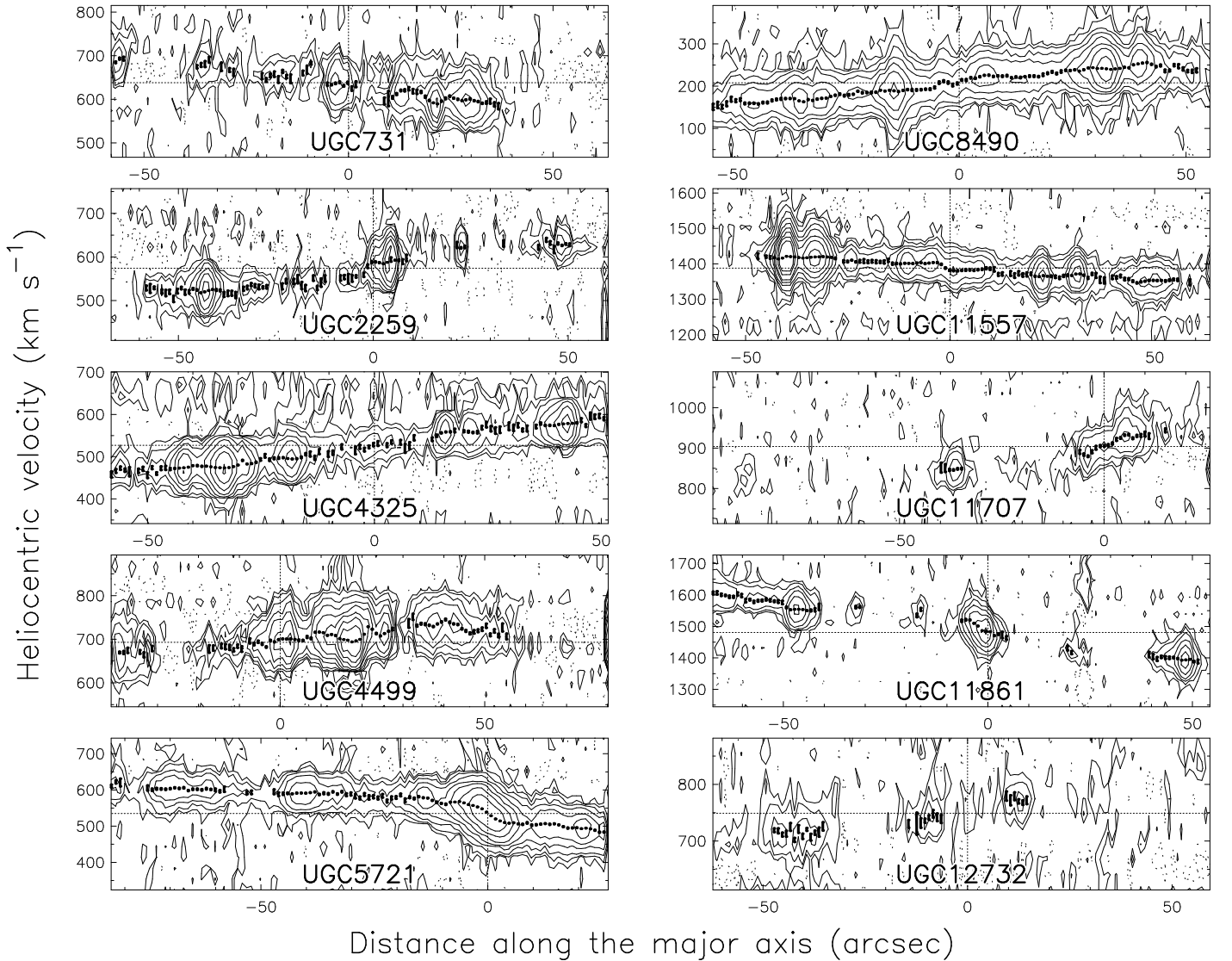


FIG. 1.— $\text{H}\alpha$  position-velocity diagrams for the 10 dwarf galaxies in our sample. The spectra have been binned to  $1''$  to increase the signal-to-noise ratio. Contour levels are  $-2, 2, 4, 8, 16, \dots$ , negative contours are dotted. The dots with error bars give the radial velocities with their formal errors as derived from Gauss fits to the velocity profiles. The vertical dotted lines indicate the galaxy centers, the horizontal dotted lines indicate the systemic velocities.

galaxies are fairly similar. Like LSB galaxies, dwarf galaxies usually have low surface brightnesses, but they may have high surface brightnesses as well (e.g., UGC 5721 and UGC 8490 in the sample presented here), and dwarf galaxies usually have smaller scale lengths than LSBs, but the selection criteria used by S99 resulted in the inclusion of galaxies with properties similar to the LSB galaxies in de Blok et al. (1996).

The observations were carried out with the Double Spectrograph at the Palomar Observatory with the 200'' Hale telescope, spread out over different observing runs, on March 2 and 3, 1997, October 26 to 28, 1998 and November 20, 1998. The March 1997 run was for a different project, and only 3 galaxies were observed from the S99 sample. Because of adverse weather conditions during the other runs, only 12 more galaxies could be observed from the S99 and de Blok (1996) samples. The observed galaxies and their global properties are listed in Table 1.

The slit width for all observations was  $1''$ , the FWHM ve-

locity resolution and the pixel size in the spatial direction are  $54 \text{ km s}^{-1}$  and  $0.5''$ , respectively. All galaxies were observed in a single 1800s exposure with the slit oriented along the major axis, at the position angle listed in Table 1. The LSB galaxies all appeared to have a well-defined nucleus, making it possible to align the slit with the center of the galaxy by eye. For the dwarf galaxies, the alignment of the slit proved more difficult, because of the diffuse, extended nature of these objects. The position of the slit was judged in relation to the galaxy image and to stars in the field of view. The systematic effects that may have been introduced by an incorrectly positioned slit are discussed in Section 6.

### 3. DERIVATION OF THE ROTATION CURVES

The data were bias subtracted, flatfielded, cleaned from cosmic ray events, wavelength calibrated, sky subtracted and continuum subtracted using standard procedures in IRAF. To increase the signal-to-noise ratio, we rebinned the spectra to  $1''$

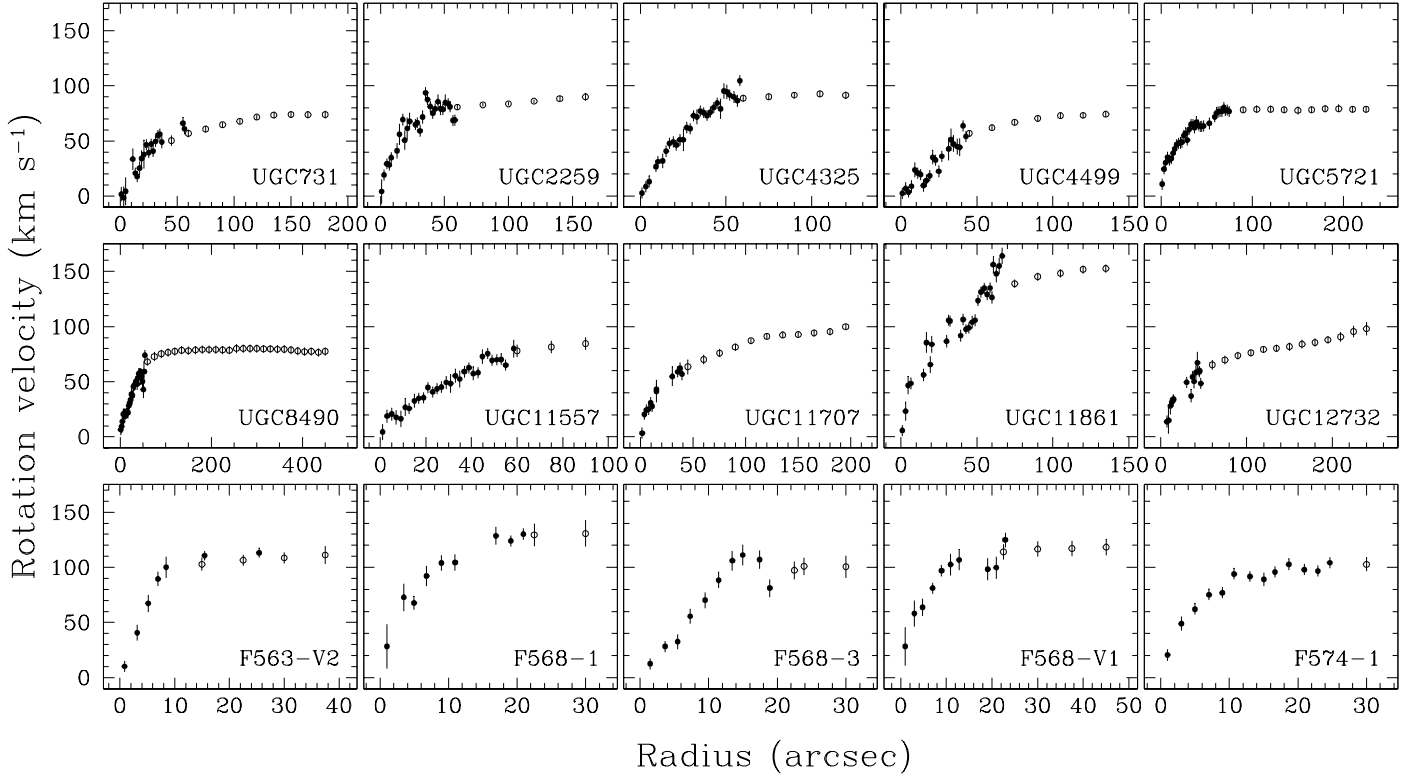


FIG. 2.— Combined  $\text{H}\alpha$ /HI rotation curves. The filled circles represent the  $\text{H}\alpha$  rotation curves as derived in this paper, the open circles are the HI rotation curves from Swaters (1999) for the dwarf galaxies and from de Blok et al. (1996) for the LSB galaxies.

pixels. The resulting  $\text{H}\alpha$  position-velocity diagrams are shown in Fig. 1. The LSB galaxies have already been presented in SMT and are not repeated here. To determine the radial velocities, we fit Gaussians to the line profiles at each position where the peak emission was higher than 3 times the noise level. These fits and their formal errors are overlayed on the  $\text{H}\alpha$  position-velocity diagrams in Fig. 1.

The position of the galaxy center along the slit was determined from the peak in the continuum. For most galaxies the continua were sufficiently bright and compact that the center could be determined to an accuracy better than  $1''$ . For a few galaxies for which the continuum was less peaked and/or fainter the position of the center was first estimated from the broad continuum peak and then refined by minimizing the differences between the receding and approaching sides of the rotation curves. The resulting shifts in the position of the center were at most a few arcseconds. The systemic velocities were determined at the position of the center and have been corrected to heliocentric velocities. In all cases they agree with the HI systemic velocities within the errors.

To determine the rotation curves, the radial velocities as determined from the Gaussian fits were folded around the center and systemic velocity. The velocity points were binned in intervals of  $2''$  (similar to the angular resolution of our observations) and averaged both in radius and velocity, weighted with the inverse square of the errors. The final error on each point of the rotation curve was defined ad hoc as half the quadratic sum of the average error of the points in the bin, weighted by the inverse square of the errors, and half the difference between the minimum and maximum rotation velocity within the bin. A minimum error of  $5 \text{ km s}^{-1}$  was imposed.

The method to derive the rotation curves as described above

is somewhat different from the method used in SMT, where the rotation velocity at each interval was estimated by eye, resulting in relatively smooth rotation curves. We have reanalyzed the SMT data with the procedure described above, so that all rotation curves presented in this paper are determined in the same way. The method used here avoids any bias or artificial smoothness that may have been introduced by determining the rotation curve by eye.

To extend the radial coverage of the rotation curves derived from the  $\text{H}\alpha$  observations, we combined them with the HI rotation curves from Carignan et al. (1988) for UGC 2259, S99 for other dwarf galaxies, and from de Blok et al. (1996) for the LSB galaxies. For the LSB galaxies there are systematic differences between the HI and  $\text{H}\alpha$  rotation curves, in the sense that the HI rotation curves appear to underestimate the rotation velocities in the inner parts (SMT, but see McGaugh, Rubin, & de Blok 2001), but the rotation velocities in the outer parts generally agree well. Hence, we replaced the inner parts of the HI rotation curves with the  $\text{H}\alpha$  data derived here. The resulting rotation curves are shown in Fig. 2.

In principle, the observed rotation curves need to be corrected for the effects of pressure, which may provide part of the support against gravity. However, as discussed in more detail in S99, these corrections are uncertain and usually small, especially in the galaxy centers. Therefore, we did not correct the observed rotation curves for asymmetric drift and we assumed that the observed rotation curves are a good representation of the circular velocities.

#### 4. MASS MODELING

Assuming that a galaxy is axially symmetric and in equilibrium, the circular velocity directly reflects the total gravitational

potential

$$-F_r = \frac{d\Phi}{dr} = \frac{v_c^2}{r}, \quad (1)$$

where  $F_r$  is the radial force,  $\Phi$  the gravitational potential,  $r$  the galactocentric radius and  $v_c$  the circular velocity. The total gravitational potential is the sum of the gravitational potentials of the individual mass components in a galaxy. Here, we assume that the galaxy consists of three main components: a stellar disk, a gaseous disk, and a spherical dark halo. Its total circular velocity is then given by:

$$v_c = \sqrt{\Upsilon_* v_d^2 + \eta v_{\text{HI}}^2 + v_h(p_1, \dots, p_n)^2}, \quad (2)$$

where  $\Upsilon_*$  is the stellar mass-to-light ratio,  $v_d$  is the rotation curve of the stellar disk for a stellar mass-to-light ratio of unity,  $\eta$  represents the inclusion of the contribution of helium to the gaseous component, assumed to be 1.32,  $v_{\text{HI}}$  is the rotation curve of the HI only, and  $v_h(p_1, \dots, p_n)$  represents the dark halo, where  $p_1$  to  $p_n$  are parameters describing its mass distribution. Each of the components in this equation is described in more detail below. The best fitting mass model for a given dark halo model is determined by fitting Eq. 2 to the observed rotation curve, with  $\Upsilon_*$  and  $p_1$  to  $p_n$  as free parameters.

#### 4.1. The stellar disk

The circular velocities due to the stellar disks have been calculated from the observed  $R$ -band luminosity profiles using the method of Casertano (1983) and Begeman (1987). For F563-V2 a  $B$ -band light profile was used. The light profiles for the dwarf galaxies have been taken from Swaters & Balcells (2002), and for the LSB galaxies from de Blok, van der Hulst, & Bothun (1995) and McGaugh & Bothun (1994). Throughout we assume that the stellar disk have a constant mass-to-light ratio  $\Upsilon_*^R$  and follow a  $\text{sech}^2$  vertical density distribution with  $z_0 = h/6$ . This particular choice for the vertical density distribution has a negligible effect on the resulting rotation curves. Finally, the surface brightness profiles of most of the galaxies in our sample are well described by a pure exponential with little or no central concentration of light, and we therefore did not include a bulge component.

#### 4.2. The gaseous disk

Circular velocity contributions from the gas disks have been computed from the radial HI surface density profiles presented in Swaters et al. (2002) and de Blok et al. (1996). All dwarf galaxies were sufficiently resolved to allow a direct determination of the radial HI surface density profile by azimuthally averaging in concentric ellipses. The LSB galaxies, however, were poorly resolved, and the radial profiles derived in this way may be affected by beam smearing (van den Bosch et al. 2000). To calculate the radial distribution of the HI for the LSB galaxies, we have used the algorithm described by Warmels (1988) that uses a iterative deconvolution scheme (Lucy 1974) to correct for the effects of beam smearing. Although the resulting density profiles may be very different, the effects on mass modeling are minor because the contribution of the HI to the rotation velocity at each radius is usually a modest fraction of the total rotation velocity. We assumed that the HI layer is infinitely thin. The choice of the vertical distribution has little effect on the resulting rotation curve. Even if the gaseous disk were to have the same thickness as the stellar disk, the difference would still be less than 5%.

#### 4.3. The dark halo

We consider two different density profiles for the dark halo: a pseudo-isothermal sphere, and a more general density distribution with variable central cusp slope.

The pseudo-isothermal sphere has frequently been used in the literature to describe the dark halo and is able to explain the observed rotation curves for a wide range of Hubble types and a wide range of stellar M/Ls (e.g., Begeman 1987, 1989; Broeils 1992a; de Blok & McGaugh 1997; Verheijen 1997; S99). Its density distribution is given by

$$\rho(r) = \rho_0 \left[ 1 + \left( \frac{r}{r_c} \right)^2 \right]^{-1}, \quad (3)$$

where  $\rho_0$  is the central dark matter density, and  $r_c$  the core radius. This density profiles gives rise to a rotation curve of the form

$$v_h(r) = \sqrt{4\pi G \rho_0 r_c^2 \left[ 1 - \frac{r_c}{r} \arctan \left( \frac{r}{r_c} \right) \right]}. \quad (4)$$

As an alternative density distribution we consider

$$\rho(r) = \frac{\rho_0}{(r/r_s)^\alpha (1+r/r_s)^{3-\alpha}}. \quad (5)$$

This density distribution changes from  $\rho \propto r^{-\alpha}$  for  $r \ll r_s$  to  $\rho \propto r^{-3}$  for  $r \gg r_s$ . For  $\alpha = 0$  the density profile thus has a constant density core and becomes comparable to that of the pseudo-isothermal sphere (at least at small radii), while for  $\alpha = 1$  it reduces to the NFW profile (Navarro et al. 1997). This ‘generalized’ NFW density distribution has previously been used in rotation curve analyses by e.g., van den Bosch et al. (2000) and vdBS. The corresponding circular velocity curve is

$$v_h(r) = v_{200} \sqrt{\frac{\mu(xc)}{x\mu(c)}}, \quad (6)$$

where  $c = r_{200}/r_s$ , with  $r_{200}$  the radius inside of which the mean density is 200 times the critical density for closure,  $x = r/r_{200}$ , and

$$\mu(x) = \int_0^x y^{2-\alpha} (1+y)^{\alpha-3} dy. \quad (7)$$

The formation of the disk within the halo leads to a contraction of the dark matter component. We assume that the collapse of the baryons within the dark halo is slow, and correct for adiabatic contraction of the halo following the procedure outlined in Barnes & White (1984), Blumenthal et al. (1986) and Flores et al. (1993). To facilitate a more direct comparison with previous studies, we do not correct for adiabatic contraction when using the pseudo-isothermal density distribution.

## 5. RESULTS

Even when the effects of beam-smearing are small, a unique decomposition of the observed RCs in terms of its contributions from the stellar disk, the gaseous disk, and the dark matter halo is hampered by uncertainties in the stellar mass-to-light ratio (the mass-to-light ratio degeneracy, e.g., van Albada et al. 1985) and by the limited spatial sampling of the the halo’s density distribution (the cusp-core degeneracy, vdBS). Below we address this non-uniqueness in the mass models by examining several extreme cases, and by analyzing the data using different methods.

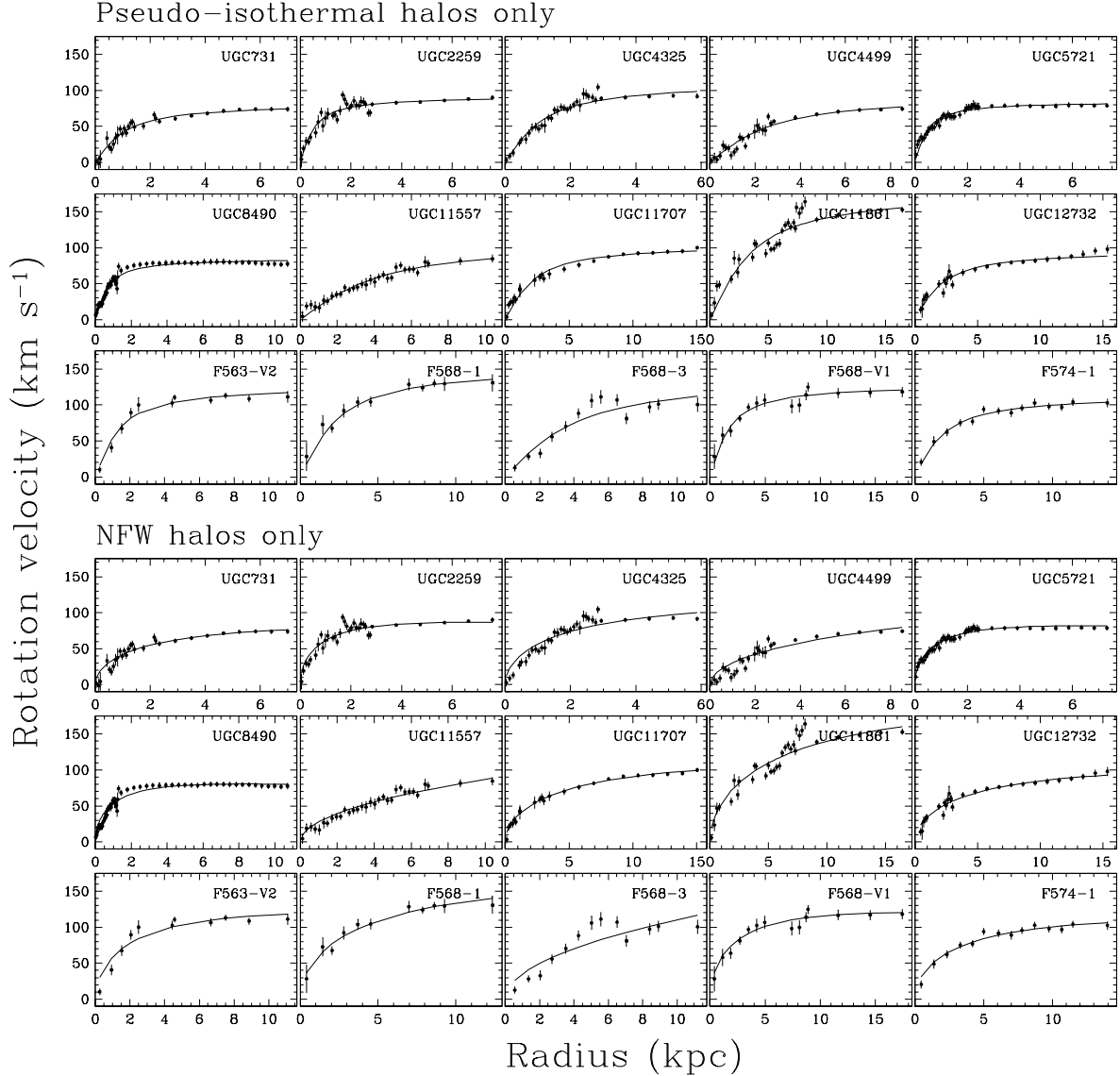


FIG. 3.— Best fitting mass models for pseudo-isothermal halo (top) and NFW (bottom). The filled circles represent the rotation curves as presented in Fig. 2, the solid lines represent the best fitting dark halos.

### 5.1. Minimum disk models

Useful limits on the dark halo properties and the slope of the dark matter density distribution can be obtained by completely ignoring the contribution of the disk (stars and gas), i.e., by assuming that the dark matter is the only mass component. These models are generally referred to as ‘minimum disk’ models.

In Fig. 3 we show the best fitting minimum disk models for both pseudo-isothermal and NFW dark matter halos. The best fitting parameters are given in Table 2. Note that for the NFW fits we impose  $c \geq 1$  to prevent models in which the scale radius  $r_s$  is larger than the virial radius of the halo. A visual inspection of the fits shows that, in most cases, both the NFW and the pseudo-isothermal halos appear able to describe the observed rotation curves fairly well. However, in a number of cases, the NFW model overpredicts the inner slope of the rotation curve: UGC 731, UGC 4325, UGC 4499, and F563-V2, and in two cases, UGC 5721 and UGC 11707, the NFW

model seems to fare better than the pseudo-isothermal model. For F568-3 and UGC 8490 both the pseudo-isothermal and the NFW give poor fits to the observed rotation curves. Overall, the pseudo-isothermal halo is somewhat more successful than the NFW halo in providing well-fitting minimum disk models for the observed rotation curves, as is also apparent from a comparison of the reduced  $\chi^2$  values (see Fig. 4). This result is in agreement with findings by other studies (Blais-Ouellette et al. 2001; dBMR; dBB).

If one assumes the disks are dynamically insignificant, and if one assumes furthermore that the dark matter has a spherically symmetric distribution, it is possible to recover the density distribution of the dark matter from the observed rotation curve in a non-parametric way. From  $\nabla^2\Phi = 4\pi G\rho$  and  $\Phi = -GM/r$  the density distribution is given by

$$\rho(r) = \frac{1}{4\pi G} \left( 2 \frac{v}{r} \frac{\partial v}{\partial r} + \frac{v^2}{r^2} \right) \quad (8)$$

This inversion method has been used by dBMBR and dBB to

TABLE 2  
BEST FIT PARAMETERS

Name (1)	maximum disk and ISO				ISO only			NFW only				
	$\Upsilon_R$ (2)	$r_c$ (3)	$\rho_0$ (4)	$\chi^2_{r,\text{max}}$ (5)	$r_c$ (6)	$\rho_0$ (7)	$\chi^2_{r,\text{iso}}$ (8)	$c$ (9)	$v_{200}$ (10)	$\chi^2_{r,\text{nfw}}$ (11)	$\alpha$ (12)	$\Delta\alpha$ (13)
UGC 731	15.1	$\infty$	1.48	1.05	0.87	163	0.90	12.0	64	1.40	0.35	0.61
UGC 2259	11.1	$\infty$	4.34	3.93	0.45	751	1.78	23.9	57	2.27	0.86	0.18
UGC 4325	8.95	...	...	1.16	0.94	263	1.46	14.8	83	3.43	0.26	0.33
UGC 4499	1.39	2.79	17.0	2.22	2.08	37.4	1.47	3.9	130	3.35	0.47	0.23
UGC 5721	2.95	1.05	123	2.22	0.39	874	2.62	24.8	53	1.54	1.16	0.17
UGC 8490	2.25	1.13	95.6	0.92	0.56	424	1.00	19.4	56	1.66	0.83	0.16
UGC 11557	1.09	$\infty$	1.48	0.74	3.35	20.0	0.67	1.0	399	0.82	0.84	0.27
UGC 11707	8.55	17.5	1.18	0.92	1.81	62.3	1.48	7.0	98	0.48	0.65	0.31
UGC 11861	5.20	9.09	0.34	3.43	2.92	69.4	4.91	8.3	159	4.67	-0.03	0.53
UGC 12732	7.06	13.9	2.17	1.02	1.77	54.7	1.11	6.8	90	0.78	-0.01	0.88
F 563-v2	5.82	...	...	0.95	1.13	231	1.36	14.4	92	4.36	0.25	0.45
F 568-1	15.8	...	...	1.71	1.95	115	0.50	10.3	129	0.62	0.67	0.12
F 568-3	1.32	4.00	20.3	2.93	3.23	35.3	2.52	1.0	637	4.97	0.38	0.19
F 568-v1	10.6	14.5	1.96	0.99	1.43	150	0.77	13.7	93	0.86	1.07	0.59
F 574-1	4.56	9.44	0.17	0.95	1.66	86.3	0.54	9.6	93	0.99	0.78	0.34

Notes — (1) the name of the galaxy. Best fit parameters for maximum disk fits with a pseudo-isothermal halo are listed in (2–5), for pseudo-isothermal halo only in (6–8), and for NFW only in (9–11). (2) gives the mass-to-light ratio in  $M_\odot/L_\odot$ . (3) and (6) list the core radius in kpc, (4) and (7) the central dark matter density in  $10^{-3} M_\odot \text{pc}^{-3}$ . (9) gives the central halo concentration index, (10) the halo velocity in  $\text{km s}^{-1}$ . (12) and (13) give the inner slope measured from the mass density profile and its error.

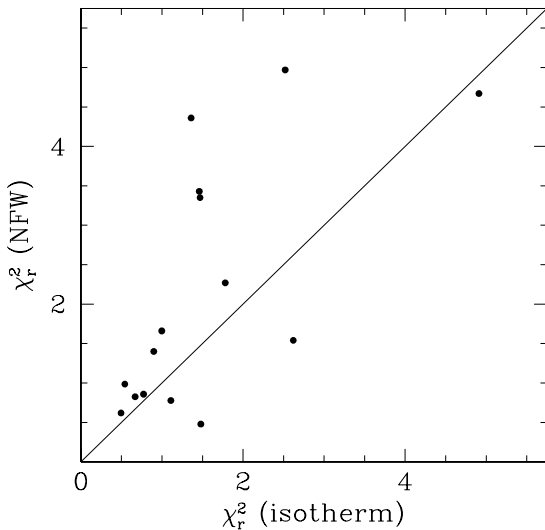


FIG. 4.— Comparison of the reduced  $\chi^2$  values for the minimum disk mass models with pseudo-isothermal and NFW halos. The solid line is the line of equality.

estimate the central cusp slopes of dark matter halos. Following their procedures, we inverted the measured rotation curve using Eq. 8, and we identified by eye a break radius inside of which we fit the density distribution with a simple power-law:  $\rho \propto r^{-\alpha_m}$ .

The derived density profiles, and the power-law slopes fit to their inner parts are shown in Fig. 5. In Table 2 the inner slopes and their uncertainties are listed. The uncertainties may be large, mostly because the derived inner slopes depend on the derivative of the rotation curves, but also because there may be little H $\alpha$  emission in the center (e.g., UGC 12732), and because the derived inner slopes may depend on only a few points with large error bars (e.g., F568-1). The distribution of measured

inner slopes  $\alpha_m$  is shown in Fig. 6. Overplotted on this distribution is the corresponding relative probability density distribution, derived by representing each entry by a normalized Gaussian centered on its value with a width given by its error, and coadding these. The measured inner slopes span a wide range with  $0 \lesssim \alpha_m \lesssim 1.2$ , and are somewhat skewed toward larger  $\alpha_m$ .

### 5.2. Mass models with disk

Although useful to obtain limits on the density distribution of the dark matter, the minimum disk models presented above are most likely not realistic. Therefore, we have also analyzed our rotation curves by including the contribution of the baryons.

We followed the approach taken by vdBS and fit mass models consisting of the generalized NFW profile of Eq. 6, the gaseous disk, and the stellar disk. For a given choice of  $\Upsilon_*$  and  $\alpha$  we determined the best fit values of  $c$  and  $v_{200}$ , taking adiabatic contraction into account, and not allowing values of  $c$  less than unity. The results are shown in Fig. 7, in which we plot  $c$ ,  $v_{200}$ , and the reduced  $\chi^2$  of the best-fit models as function of  $\alpha$  for four different values of the stellar mass-to-light ratio  $\Upsilon_* = 0$ , 0.5, 1.0, and 2.0, but only if those values are lower than the maximum disk  $\Upsilon_*$  as listed in Table 2. This covers the typical range of mass-to-light ratios expected from stellar population modeling (e.g., Worthey 1994; Bell & de Jong 2001).

A number of general trends are apparent. The halo concentration  $c$  of the best fitting model decreases with increasing  $\alpha$ , because the enclosed mass for the different models has to be similar. The value of  $v_{200}$  reaches a maximum where  $c = 1$ . For steeper  $\alpha$ , the best fitting  $c$  would be smaller than unity for which, as mentioned above, Eq. 5 no longer gives a meaningful description of the dark matter distribution. As a consequence, the quality of the fits rapidly decreases. Finally, an increase of  $\Upsilon_*$  causes  $c$  to decrease, because more and more of the inner rise of the rotation curve is due to the stellar disk. For most galaxies the quality of the fit is similar for cusp slopes in the

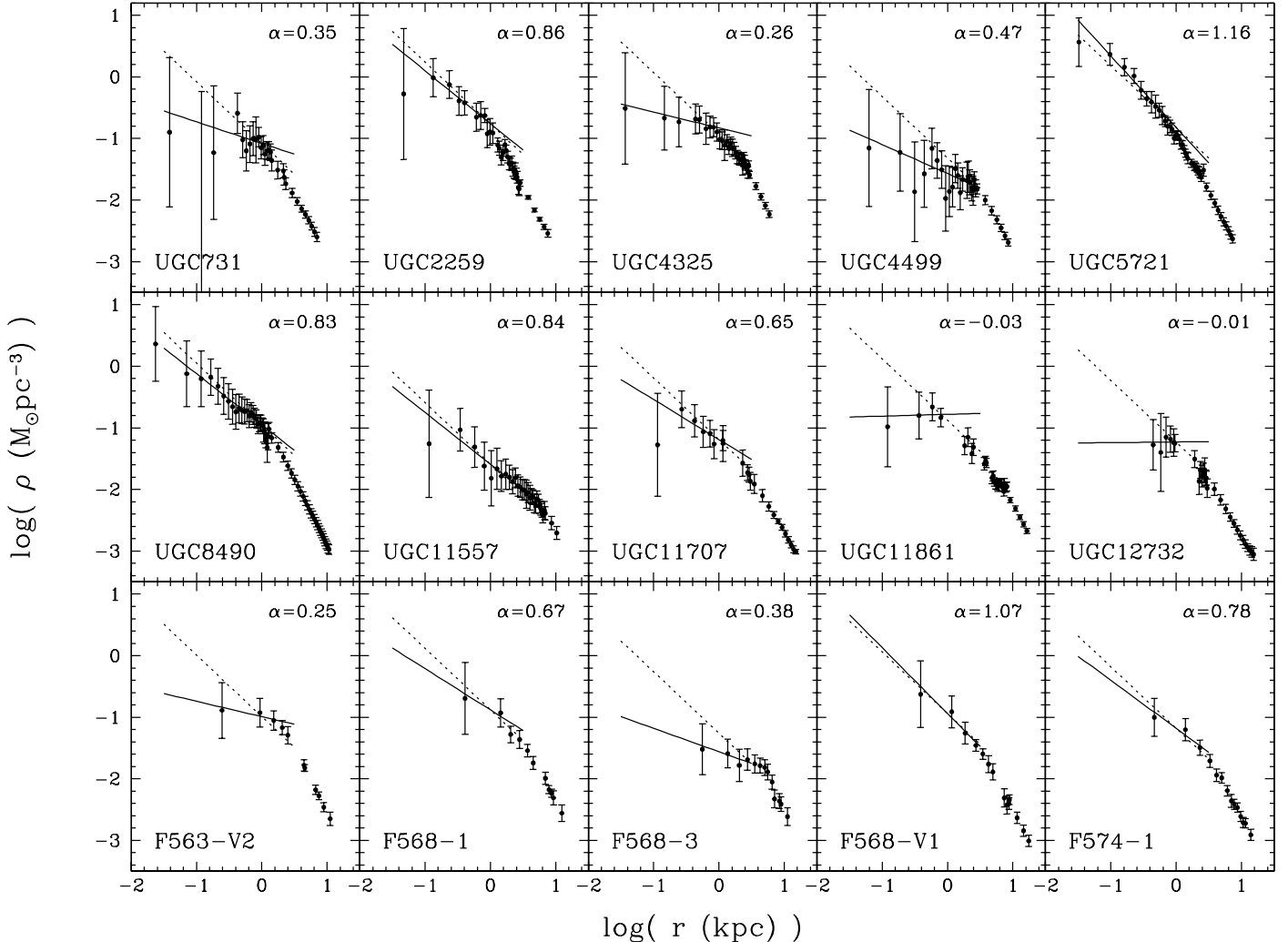


FIG. 5.— Log-log plots of the density distribution as derived by inverting the observed rotation curves, following the procedure as described in Section 5.1. The solid line represents a weighted least-squared fit to the parts of the profile within the break radius, the dotted lines represent a slope of  $\alpha = 1$ .

range  $0 \lesssim \alpha \lesssim 1.0$ . Only for four galaxies in our sample do models with  $\alpha = 0$  yield significantly better fits than for  $\alpha = 1$  independent of  $\Upsilon_*$  (UGC 4325, UGC 4499, F563-V2 and F568-3). Finally, for  $\alpha \gtrsim 1.0$ , the quality of the fit decreases rapidly for virtually all galaxies.

These results are similar to those of vdBS, who fitted the same mass models but to the HI rotation curves only. For the galaxies in common with vdBS (all UGC galaxies except UGC 2259, UGC 5721 and UGC 11557) the results presented here are similar, suggesting that our higher resolution H $\alpha$  data have not strongly reduced the degeneracy in the mass models. Two exceptions are UGC 11861 and UGC 12732 for which  $\alpha$  has become better constrained with the new H $\alpha$  data.

In summary, even with the high-resolution H $\alpha$  data presented here a unique decomposition of the rotation curves is not possible. In particular the freedom in the inner slope of the dark matter distribution is large, and most galaxies *individually* are consistent with mass models with inner slopes in the range  $0 \lesssim \alpha \lesssim 1$ . However, for  $\alpha > 1$  the quality of the fits decrease rapidly, and inner slopes with  $\alpha = 1.5$  are clearly inconsistent with the observations.

## 6. OBSERVATIONAL EFFECTS

Previous studies have found that the H $\alpha$  and HI rotation curves of dwarf and LSB galaxies are consistent with the picture that all dark matter halos have constant density cores and that pseudo-isothermal halos in general provide better fits to the rotation curves than the cuspy NFW halos. The results presented in Section 5 are consistent with these findings. However, there are various systematic effects that may affect the derived inner slope, such as beam smearing, slit alignment errors, line-of-sight projection effects and non-circular motions. Clearly, such systematic effects need to be considered before intrinsically steep slopes can be ruled out observationally.

### 6.1. Beam smearing

The effect of beam smearing is to dilute steep velocity gradients, thus leading to an underestimate of the inner slope in the derived rotation curves. Previous attempts to constrain the central mass density of LSB galaxies using HI rotation curves with a typical resolution of  $15''$  to  $30''$  suffered strongly from beam smearing effects. The H $\alpha$  observations presented here have a much higher spatial resolution, of about  $1''$  to  $2''$ , and

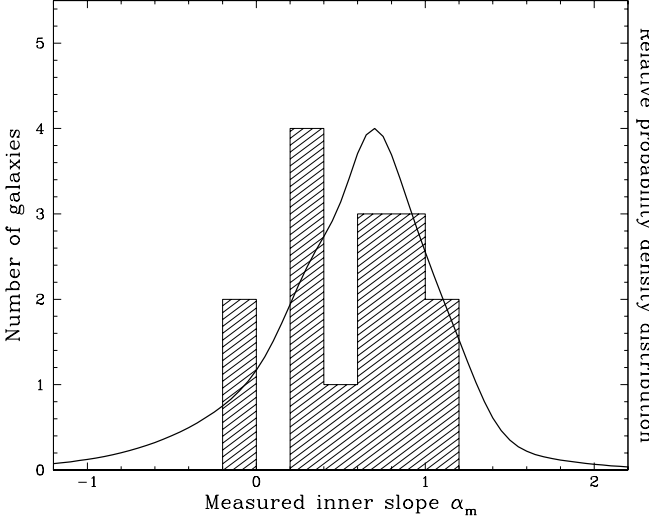


FIG. 6.— Histogram of measured inner slopes  $\alpha_m$ . The solid line is the corresponding relative probability density distribution.

clearly beam smearing will play a less dramatic role. However, the measurement of the inner slope usually depends on the very inner points of the rotation curves, and hence beam smearing as a result of seeing still needs to be considered, especially for galaxies at large distances.

### 6.2. Slit width

For a larger slit width, a larger fraction of the velocity field is encompassed by the slit. The projected rotation velocities away from the major axis are lower than those on the major axis, especially near the center of the galaxy. This skews the observed line profile toward lower rotation velocities, and hence a wide slit may lead to an underestimate of the inner slope.

### 6.3. Slit alignment errors

A misalignment of the slit may happen either in position or in position angle. The latter is likely to be negligible, both because position angles can usually be measured accurately, and because even large errors in position angle will still only have a small effect on the rotation curve. A much more important effect is an offset between the position of the slit and the center of the galaxy. As a result of such an offset, the steepest gradient in the velocity field will be missed, resulting in an underestimate of the inner slope. There are three main reasons for offsets: observational errors, uncertainties in the position of the galaxy centers, and differences between the kinematic and optical centers.

The observational errors depend on the method used to align the slit with the galaxy image. Here, we have aligned the slit visually, because most galaxies were clearly visible on the slit viewing camera. For the LSB galaxies, we estimate that we could align the slit with an accuracy of around  $1''$ . For the dwarf galaxies the alignment was more difficult, because of their diffuse and extended nature, and the error in the alignment will likely be larger. A better method to position the slit would be to use the coordinates of the optical center, e.g., like dBB have done. They find that telescope control usually allows a repeatable positioning with an accuracy of better than  $1''$ . Their procedure reduces the observational uncertainty significantly.

Another contributor to the alignment error is the accuracy of the optical center itself. For many catalogued galaxies the optical

center has been determined from photographic plates. For the faint and often irregular dwarf and LSB galaxies, the centers determined in this way may well be incorrect by many arcseconds. But even if CCD photometry with accurate astrometry is available, there may still be considerable uncertainty in the position of the optical center. Swaters & Balcells (2002) have determined the centers of the 171 dwarf galaxies in their sample, and published the centers of the isophotal fits versus radius. Their figures show that there is considerable spread in the best fitting centers as a function of radius, and that the centers of the inner and outer isophotes usually differ by a few arcseconds, and sometimes even as much as  $30''$ .

A third possible contributor to slit alignment errors is an offset between the kinematical and optical centers. Such an offset is not uncommon in dwarf and LSB galaxies (e.g., Puche, Carignan, & Wainscoat 1991; Swaters et al. 1999). Obviously, if the dynamical and the kinematical center do not agree, the steepest gradient in the velocity field of the galaxy may be missed, and the inner slope underestimated. Unfortunately, without two-dimensional velocity fields it is not possible to assess whether an offset between kinematical and optical center is present.

### 6.4. Edge-on galaxies

In edge-on galaxies, the line-of-sight traverses the entire galaxy disk, and hence a range of radii contribute to the observed velocity profiles. However, only the gas on the major axis reflects the circular velocity at that galactocentric radius, whereas gas from all other radii has smaller projected velocities. The result is a broad velocity profile that is strongly skewed toward lower rotation velocities. Simply taking the barycenter or a Gaussian fit will thus result in an underestimate of the rotation velocity. To derive the true rotation velocity, the extreme velocity should be used. To determine this reliably a very high velocity resolution is needed, much higher than is provided by the long-slit observations presented here. In addition, determining the extreme velocity becomes more difficult if the  $H\alpha$  emission is weak on the line of nodes.

### 6.5. Distribution of $H\alpha$

A more subtle cause of uncertainties in determining the dark matter cusp slope is related to the spatial distribution of  $H\alpha$  in the part of the galaxy that is visible through the slit. If the  $H\alpha$  emission is uniform, this is not likely to play a role, but if the  $H\alpha$  distribution is knotty, substantial underestimates may occur. For example, consider the case in which there is no  $H\alpha$  emission on the major axis, but that there is emission just next to it, but still within the area viewed by the slit, or smeared into that area by the seeing. The projected rotation velocity just next to the major axis is lower than exactly on the major axis, and thus an irregular distribution may lead to an underestimate of the derived rotation curve. This effect is stronger when the seeing is poor, and it is especially strong in the center, where small spatial differences may lead to large velocity differences (see also Barth et al. 2001). The effects of the distribution of  $H\alpha$  can be modeled if an  $H\alpha$  image is available, allowing a more accurate measurement of the rotation curve.

### 6.6. Non-circular motions

Non-circular motions are another source of systematic errors in the mass densities derived from rotation curves. The usual assumption for derived rotation curves is that the gas moves on

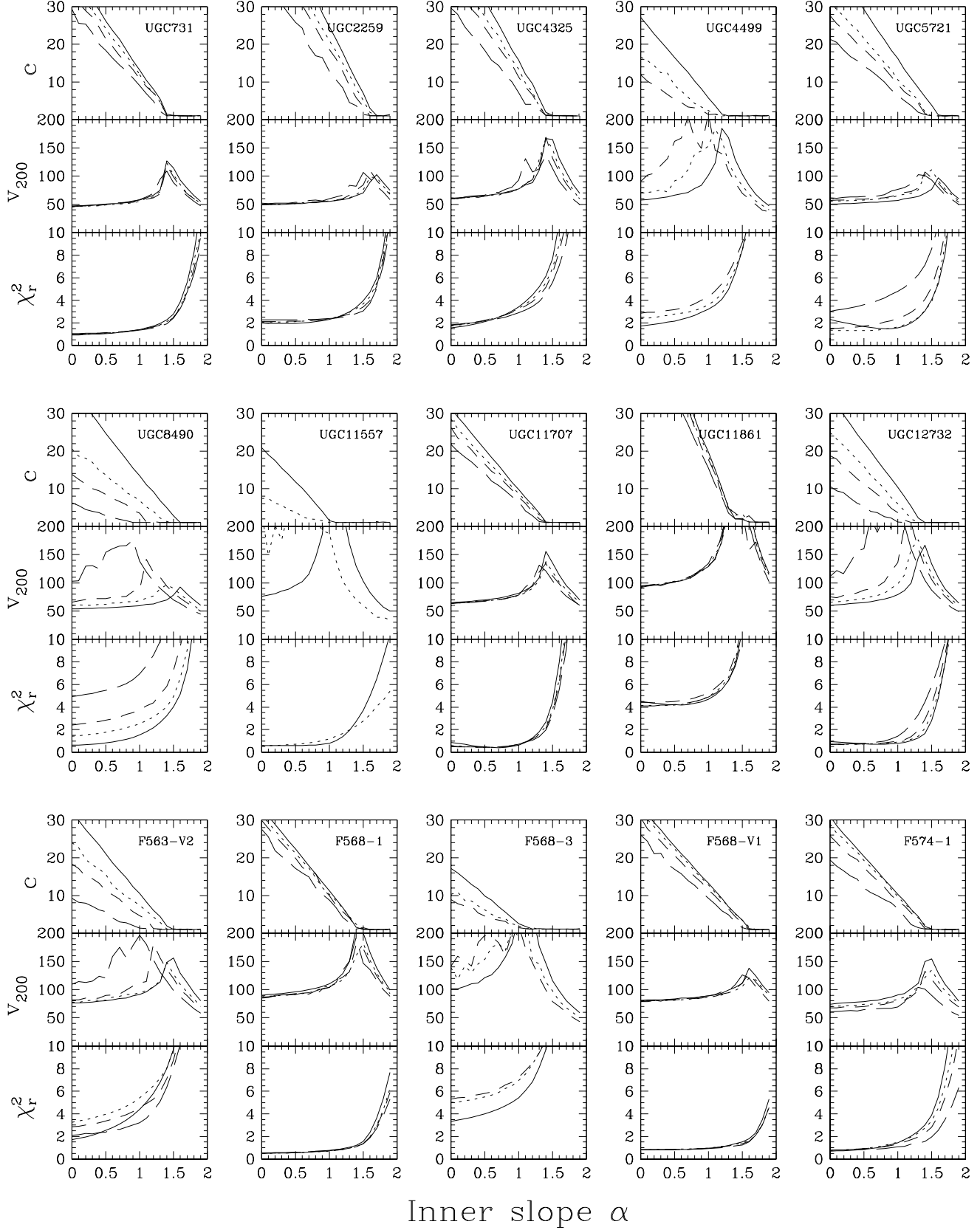


FIG. 7.— Best fitting parameters and  $\chi^2_r$  for the generic halo fits. The top panel for each galaxy shows  $c$  versus  $\alpha$ , the middle panel  $V_{200}$ , and the bottom one  $\chi^2_r$ . The different lines represent fits with different  $\Upsilon_*$ , where the solid line represents  $\Upsilon_* = 0$ , the dotted line is  $\Upsilon_* = 0.5$ , the short dashed lines is  $\Upsilon_* = 1$  and the long dashed line is  $\Upsilon_* = 2$ .

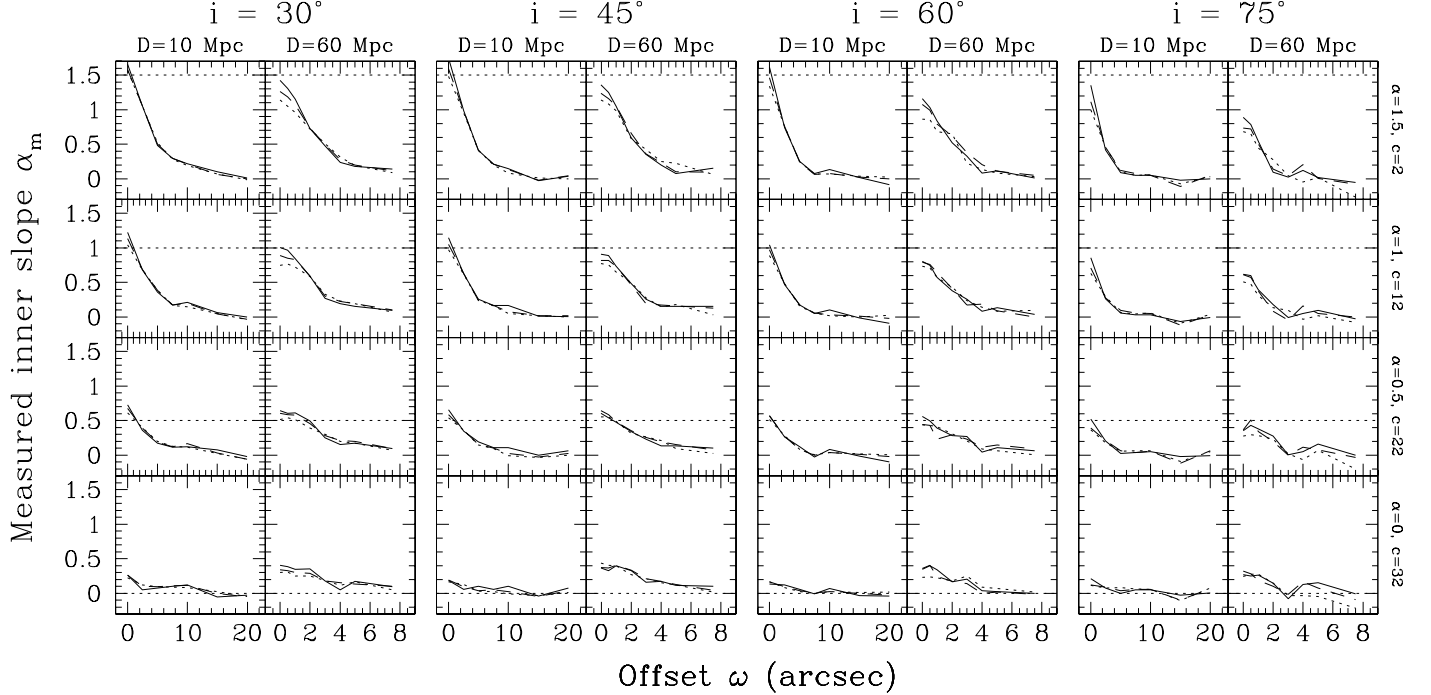


FIG. 8.— The inner slope  $\alpha$  as derived from the model observations versus the offset of the slit from the major axis  $\omega$ , for model galaxies at 10 Mpc and 60 Mpc, and a range of inclinations as indicated above each column. The solid line represents the results for a seeing of  $1''$ , the dashed line the results for  $1.5''$ , and the dotted line the results for  $2''$ . The horizontal dotted lines represent the intrinsic inner slope of each model.

circular orbits. However, this assumption is not always accurate. Structural features such as bars, spiral arms, lopsidedness, the irregular distribution of stars and gas, and the effects of star formation may all leave an imprint on the kinematics. The effects of such non-circular motions are usually most important in the central regions, where rotation velocities are relatively low and were the physical causes for non-circular motions, such as bars and star formation activity, are strongest.

It is difficult to model the effect of non-circular motions on the derived rotation curve because many factors may contribute. For example, a high star formation rate may lead to gas outflows and to an increase the dispersion of the emission line gas, or of the gas clouds, resulting in a lower azimuthal velocity component, and hence an underestimate of the rotation velocity. The magnitude of this asymmetric drift is uncertain and difficult to calculate, as was pointed out in Section 3. The effects of bars on the rotation curves depend on the bars' properties such as their orientation and strength. Other structural perturbations such as lopsidedness or spiral structure, may either lead to an underestimate or an overestimate of the rotation velocity, depending on the kind of disturbance and its orientation.

## 7. MODELING

From Section 6 it is clear that there are strong observational biases toward shallower slopes. In this Section, we derive more quantitative estimates of how these observational effects affect the inner slopes derived from inversion of the rotation curves and the mass modeling, based on model observations. We focus on the effects of the seeing, slit width, slit alignment errors and edge-on galaxies, because their effects can be most readily determined from model observations.

To construct the model velocity fields, we have assumed the model galaxies to be infinitely thin disks that are uniformly

filled with  $\text{H}\alpha$  emission. We also experimented with alternative, more complicated distributions, but found that these do not significantly change the main results as long as the size of the seeing disk is small compared to the typical length scale of variations in the  $\text{H}\alpha$  emission. We assumed that the model galaxies are dominated by their dark matter halos, and we considered dark matter halos with a density distribution given by Eq. 5, with  $\alpha=0, 0.5, 1$ , and  $1.5$ . The model with  $\alpha=1$  has  $c=12$  and  $v_{200}=75 \text{ km s}^{-1}$ . For the other models, the values of  $c$  and  $v_{200}$  were determined from a best fit to the  $\alpha=1$  model, to ensure that the rotation curves are similar in shape. Each model was placed at a distances of 10 Mpc and 60 Mpc, and at inclinations of  $30^\circ, 45^\circ, 60^\circ$  and  $75^\circ$ .

After we constructed each model, it was convolved with the seeing and the velocity dispersion. We made models for three different values of the seeing,  $1'', 1.5'',$  and  $2''$ , and assumed that the model velocity dispersion is dominated by the instrumental one, as is also the case for the galaxies in our sample. Next, we extracted from the model velocity field a spectrum for a given slit width and a given offset from the model galaxy center, and derived a rotation curve using the same procedure as for the real observations. Because the effects of seeing and slit width are similar, and because usually observers match the slit width to the typical seeing, we have focused only on models with equal slit width and seeing. Finally, we analyzed these model rotation curves in the same way as the real data (see Section 5). The results are described in detail below.

### 7.1. Inversion of the rotation curve

We measured the inner slope by inverting the model rotation curves using Eq. 8, and following the same method as outlined in Section 5.1. The results for model galaxies with intrinsic inner slopes of  $\alpha=0, 0.5, 1$  and  $1.5$  are shown in Fig. 8, in which

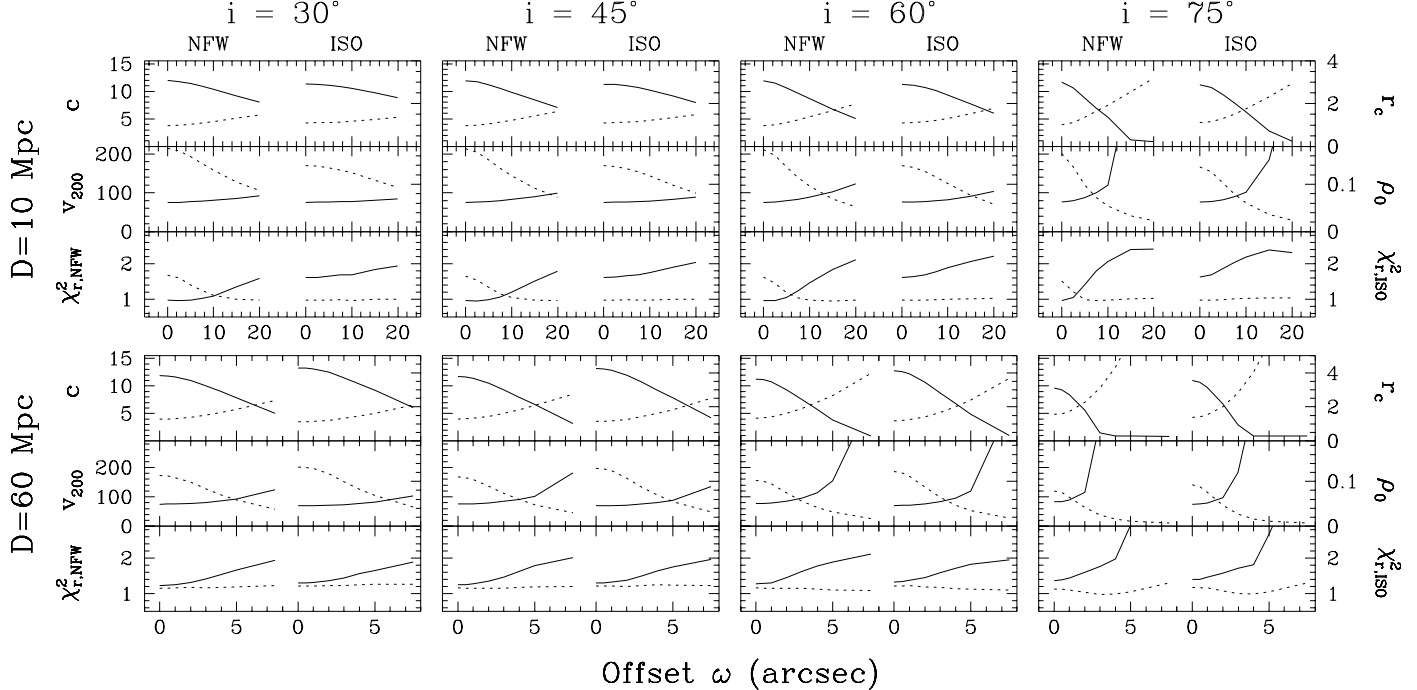


FIG. 9.— Parameters for the best fitting mass models fitted to a model with an NFW halo with  $c = 12$  and  $v_{200} = 75 \text{ km s}^{-1}$  (left column in each panel) and a pseudo-isothermal halo with  $r_c = 1.1 \text{ kpc}$  and  $\rho_0 = 0.14 \text{ M}_\odot \text{ pc}^{-3}$  (right column in each panel). The solid lines give the resulting parameters for an NFW fit, the dotted lines for a pseudo-isothermal fit, both plotted versus the offset between the slit and the major axis of the galaxy. The results are virtually independent of seeing, and hence we only show the model for a seeing of  $1''$ .

the measured inner slope  $\alpha_m$  is plotted as function of slit offset  $\omega$  for inclinations  $30^\circ, 45^\circ, 60^\circ$ , and  $75^\circ$ , and for distances of 10 and 60 Mpc. The results are shown for models with a seeing of  $1''$  (full line),  $1.5''$  (dashed line), and  $2''$  (dotted line). The horizontal dotted line in each panel represents the intrinsic inner slope of each model.

If the slit is properly aligned with the major axis, i.e.,  $\omega = 0''$ , the inner slope can be accurately retrieved for the galaxies at 10 Mpc, i.e., the effects of seeing and slit width are negligible, provided that  $i \lesssim 60^\circ$ . For galaxies with inclinations around  $75^\circ$ , the inner slope is significantly underestimated for the model galaxies with intrinsically steep slopes, and this underestimate is larger for poorer seeing.

For the model galaxies at 60 Mpc, however, the effects of slit width and seeing play a role at all inclinations. Even at low inclinations and small seeing disks, the inner slopes may be significantly underestimated. For example, for model galaxies with  $\alpha = 1$ , the inner slope is underestimated by around 20% for  $i = 60^\circ$ , and around 40% for  $i = 75^\circ$ . Note that for galaxies with shallow intrinsic slope the measured inner slope is actually an overestimate of the intrinsic inner slope. As was also pointed out by dMBMR, for these galaxies the innermost points already include the parts where the density distribution turns over from its more shallow inner parts to the steep  $r^{-2}$  outer parts.

Fig. 8 also shows that, if the slit is not aligned correctly with the major axis, the measured inner slope may be severely underestimated, both for  $D = 10 \text{ Mpc}$  and  $D = 60 \text{ Mpc}$ , for galaxies with rotation curves with steep intrinsic slopes. As the offset increases, the velocity gradient over the slit becomes more shallow, and for large offsets the measured inner slope may even resemble a constant density core. Note that the effect of slit offsets does not scale linearly with distance. For example, for

the model galaxy with  $D = 60 \text{ Mpc}$ ,  $i = 45^\circ$ , and  $\alpha = 1$ , a measured inner slope of  $\alpha_m \approx 0.6$  is found for  $\omega = 2''$ . One might expect a similar value of  $\alpha_m \approx 0.6$  for  $\omega = 12''$  for the same model at  $D = 10 \text{ Mpc}$ , but instead it occurs at about  $\omega = 3''$ . This is a result of the sampling in combination with the definition of a break radius. For galaxies at smaller distances, the inner parts of the rotation curves are well sampled, and the effects of an offset become noticeable in the derived density distributions even for small offsets. For galaxies at large distances, the inner parts of the rotation curves are more poorly sampled, and larger offsets are required to cause a noticeable change in the density distribution.

In order to get a clear picture of the systematic effects as a result of seeing, slit width and offsets, we have not included realistic errors on the rotation curves. The scatter seen in Fig. 8 is the result of discretisation noise in the models. We have repeated the modeling and added Gaussian noise to the rotation velocities with an amplitude of  $5 \text{ km s}^{-1}$ . This results in a typical error on the measured inner slope  $\alpha_m$  of 0.25.

## 7.2. Mass model fitting

We have fitted mass models to the rotation curves derived from the models for different values of the offset  $\omega$ , seeing, and slit width, in order to investigate how accurately the halo parameters can be retrieved. In these fits, the intrinsic inner slope was kept fixed because for realistic errors on the derived rotation velocities the cusp-core degeneracy prevents an accurate determination of the inner slope, as is clear from the general dark matter fits presented in Fig. 7 and from the models presented in vdBS. We focused on the NFW halo (which has  $\alpha = 1$ ) and the pseudo-isothermal halo (which has  $\alpha = 0$ ), since these are most often used in the literature.

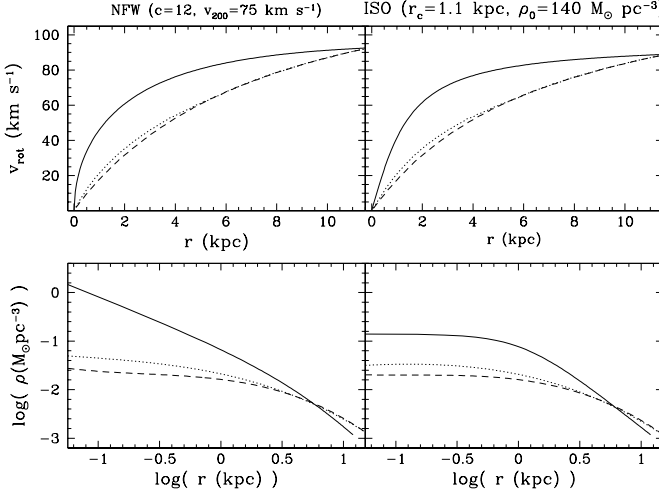


FIG. 10.— The top panels show the input rotation curve (solid lines) and the rotation curves as derived from the model observations of an edge-on galaxy with  $1''$  seeing, for a constant density distribution (dashed lines) and an exponentially declining distribution (dotted lines). The bottom panels show the input and the derived density distribution, with the line coding the same as in the top panel. The left column gives the results for an NFW halo, the right model for a pseudo-isothermal halo. The halo parameters are given above each column.

We assumed that the model galaxies are dominated by either an NFW halo with  $c = 12$  and  $v_{200} = 75 \text{ km s}^{-1}$ , or a pseudo-isothermal halo with  $r_c = 1.1 \text{ kpc}$  and  $\rho_0 = 110 \text{ M}_\odot \text{ pc}^{-3}$ . We fit both pseudo-isothermal and NFW halos to both sets of models, for the same range in seeing, slit width, offsets and inclination used in Section 7.1, and for distances of 10 Mpc and 60 Mpc. For all galaxies, we considered the model rotation curves out to a maximum radius of 10 kpc. To mimic the properties of the observed rotation curves as closely as possible, we have resampled the model rotation curves in the same way as the observed ones. For the model galaxies at 10 Mpc, the rotation curves were sampled every  $2''$  in the inner 3 kpc, and every  $15''$  at larger radii. This closely resembles the combination of H $\alpha$  and HI data for the closeby galaxies. The model galaxies at 60 Mpc were sampled every  $2''$  out to the last measured point. We have added Gaussian noise to the rotation curves with  $\sigma = 5 \text{ km s}^{-1}$ .

In Fig. 9 we present the results. In each panel, the left column shows the fits to the models built from an NFW halo, and the right column shows the fits built from a pseudo-isothermal halo. Each model has been fit both with an NFW halo (full line) and a pseudo-isothermal sphere (dotted line). As can be seen in Fig. 9, the input parameters can be retrieved fairly accurately if the slit is aligned with the major axis, and if the rotation curves are fit with the correct model. We found that the effects of seeing and slit width are generally negligible, and therefore we only show the results for a seeing of  $1''$  in Fig. 9. Seeing and slit width start to play a minor role in the model galaxies at 60 Mpc and with inclination  $i \gtrsim 60^\circ$ , in which case errors in the derived parameters of up to about 10% may occur.

If the slit is not correctly aligned with the major axis, much larger errors are introduced. At 60 Mpc, an offset of a few arcseconds is sufficient to lead to a significant error in the derived parameters, especially for highly inclined systems. At 10 Mpc, the impact of slit offsets is much less pronounced, and the derived parameters are hardly affected even for offsets as large

as  $5''$ , except in highly inclined systems, where the effects become significant for smaller offsets. Overall, the results derived from mass modeling are less sensitive to the effects of seeing, slit width, and slit offsets than the results from rotation curve inversion. This is expected, because the entire rotation curve is used to fit the mass models, whereas only the inner parts of the rotation curve, which are most affected by seeing, slit width, and slit offset, are used to determine the inner slope.

To investigate the usefulness of  $\chi^2$  as a discriminator between the two mass models, we have calculated and plotted the  $\chi^2$  values for both the NFW and the pseudo-isothermal halos. For galaxies at small distances, the  $\chi^2$  appears to be a useful discriminator. If model galaxies with pseudo-isothermal halos are fit with NFW halos, the fits are poor. The same is true for the converse, although for large slit offsets the pseudo-isothermal fits to the NFW models may lead to the incorrect conclusion that these models have pseudo-isothermal halos. The required offsets are large and unrealistic, except perhaps in galaxies with high inclinations. At a distance of 60 Mpc, the value of  $\chi^2$  is not a useful discriminator. Even if the slit is well aligned with the major axis, the  $\chi^2$  values for both models are comparable. If the slit is somewhat offset from the major axis, the pseudo-isothermal fits consistently result in lower  $\chi^2$  than the NFW models, even if the intrinsic halo shape is NFW. To be able to reliably distinguish between the models presented here, errors on the rotation velocities of about 1 or 2  $\text{km s}^{-1}$  are needed. Given the often weak H $\alpha$  emission, and the likely presence of small and large-scale non-circular motions, it seems unlikely that the circular velocity can be derived with sufficient accuracy.

### 7.3. Edge-on galaxies

As mentioned in Section 6.4, projection effects may strongly affect the derived rotation curves for galaxies that are seen close to edge-on. Here, we show two models to illustrate the systematic effects.

Because the line of sight traverses the entire disk in edge-on galaxies, the results will depend somewhat on the adopted radial distribution of the H $\alpha$  emission, and we therefore constructed two sets of models, one with constant level of H $\alpha$  emission, and one with a radially exponential decline. As before, we assumed the galaxies are dominated by their dark matter halos, and we used the same halo models as in Section 7.2. The model galaxies were placed at a distance of 10 Mpc, at an inclination of  $90^\circ$ , and “observed” with a  $1''$  slit and  $1''$  seeing. Finally, the rotation curves are derived using the same procedure as used for the real observations, i.e., by fitting Gaussians to the line profiles. We have also used the barycenter to derive the rotation curve, and this gives virtually identical results.

In Fig. 10 we compare the input model rotation curves (solid lines) to the ones derived from the edge-on model galaxies. In addition, we compare the input density distributions with those obtained from the inversion of the model rotation curves, using Eq. 8. Dashed (dotted) lines correspond to models with a constant (exponentially declining) level of H $\alpha$  emission. From Fig. 10 it is clear that for edge-on galaxies the rotation curves derived from long-slit observations using traditional methods suffer from extremely strong systematic effects. Hence, the dark halo parameters derived from these rotation curves are likely to be inaccurate.

## 8. DISCUSSION

8.1. *Limits on the inner slopes*

Our results presented in Section 5, based both on a measurement of the inner slope by inversion of the observed rotation curve and on fitting mass models, have shown that the measured inner slopes derived for the galaxies in our sample span a wide range from  $\alpha_m \sim 0$  to  $\alpha_m \sim 1.2$ . Taken at face value, the fact a substantial fraction of the galaxies in our sample have a measured inner slope around zero may lead to the conclusion that these galaxies cannot have cuspy inner slopes. However, as discussed in Section 6, there are many systematic effects that may affect the measured inner slopes, and most of these will lead to an underestimate. We will now use the modeling results from Section 7 to try and determine which range of intrinsic inner slopes is consistent with the range in measured inner slopes. We will only consider the range  $0 < \alpha \lesssim 1$ . Slopes steeper than  $\alpha = 1.5$  are ruled out by the observations presented here, and by several previous studies (e.g., dBMBR; vdBS).

8.1.1. *Inner slopes from mass density profiles*

In Fig. 11 we show the distributions of measured inner slopes for the galaxies in our sample with  $v_{\text{sys}} \leq 2000 \text{ km s}^{-1}$  (which have distances more typical of the model galaxies at 10 Mpc, presented in Section 7) and with  $v_{\text{sys}} > 2000 \text{ km s}^{-1}$  (which have distances more typical of the model galaxies at 60 Mpc). We will refer to these subsamples as the 10 Mpc and the 60 Mpc sample. Overplotted on the histograms are the expected distributions for different intrinsic inner slopes of the dark matter distribution, for different values for the error in the slit position, and a slit with of  $1''$  (the slit width that we used in our observations). The expected distributions have been calculated as follows. From our modeling results presented in Fig. 8, we know for each model halo with intrinsic inner slope  $\alpha$  what the measured inner slope  $\alpha_m$  will be for a given offset. Assuming a Gaussian distribution for the slit positioning error  $\sigma_{\text{off}}$ , we can also calculate the probability that a particular  $\alpha_m$  will be measured. While calculating this probability distribution we assumed that  $\alpha_m$  can be measured with no observational error. However, in our observations we found a typical error on the measured inner slope of 0.25 (see Table 2). To compare the expected distribution of  $\alpha_m$  with the observed one, we have therefore convolved the expected one with a Gaussian with  $\sigma_m = 0.25$ . Finally, we selected for each galaxy the model with the inclination closest to the inclination of that galaxy, and we averaged the probability distributions for all galaxies in our sample to produce the expected distributions shown in Fig. 11.

For each adopted halo model we show the expected distributions for different values of the offset error. It is uncertain what the actual amplitude of the slit offset error is, given that telescope pointing errors, uncertain positions of the galaxy centers, and possible offsets between the morphological and dynamical center all may play a role. Therefore, we plot several expected distributions for different values of the offset error  $\sigma_{\text{off}}$ . The solid lines give the distributions of measured inner slopes expected if galaxies are dominated by halos that have inner slopes  $\alpha = 1$  and offset errors of  $0'', 1'',$  and  $2''$ , as indicated above each curve. The distributions expected if galaxies are dominated by halos with inner slopes  $\alpha = 0$  are almost insensitive to the offset errors, because any offsets will result in a measured inner slope close to zero (see bottom row in Fig. 8). Hence, we only show one curve for the  $\alpha = 0$  case.

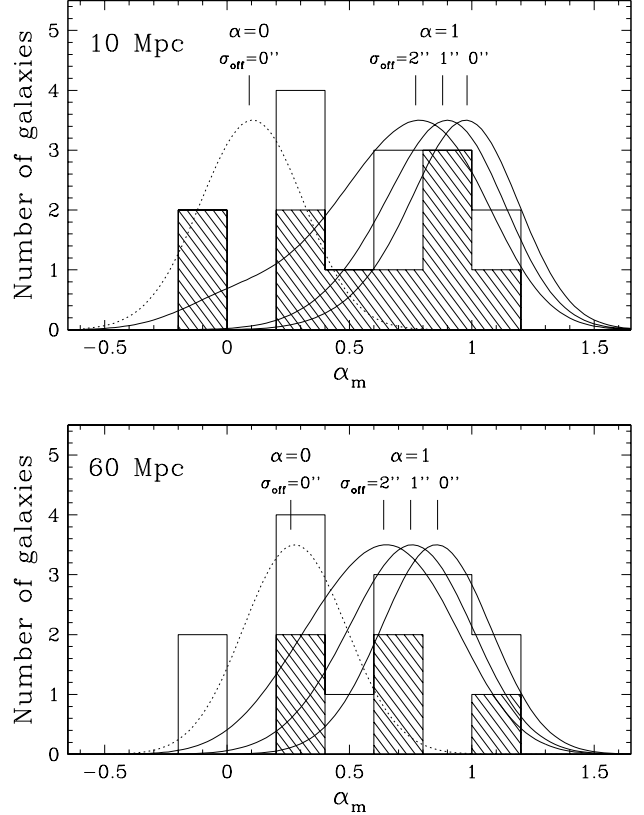


FIG. 11.— The unshaded histograms in both panels represent the distribution of inner slopes derived from fits to the central parts of the density profiles as given in Fig. 6. The shaded area indicates the galaxies in the distance group as indicated in the top left of each panel. The bell-shaped curves represent the expected distribution of measured inner slopes for the adopted intrinsic inner slope  $\alpha$  and slit alignment error  $\sigma_{\text{off}}$  as labeled above each curve. A slit width of  $1''$ , a seeing of  $1''$  and a measurement error on  $\alpha_m$  of 0.25 was assumed. How these curves were derived is explained in the text.

A comparison of the expected distribution with the observed one is difficult, because of the small number of galaxies, especially in the 60 Mpc sample. Still, it seems that the expected distribution for  $\alpha = 0$  appears inconsistent with the observed one, both in the 10 Mpc and 60 Mpc samples. In both cases, there appear to be too many galaxies with high  $\alpha_m$ . The expected distribution based on models with  $\alpha = 1$  is in reasonable agreement with the number of galaxies with steep measured inner slopes, but it underpredicts the observed number of galaxies with shallow inner slopes in the 10 Mpc sample if  $\sigma_{\text{off}}$  is small. About 25% of the galaxies in our sample appear to have  $\alpha_m$  inconsistent with  $\alpha = 1$ , unless the alignment error is larger. If  $\sigma_{\text{off}}$  is about  $2''$ , one expects to observe a wide range in  $\alpha_m$ , even as low as  $\alpha_m = 0$ , and the expected distribution is fairly consistent with the observed one.

It appears that the observed distribution of measured inner slopes in the 10 Mpc sample is not uniquely consistent with any of the models overplotted. This may simply be the result of the small number of galaxies in our sample. Alternatively, it could be that one or more of our assumptions does not hold, e.g., non-circular motions may play a role, the mass distribution may not be spherical, or the stellar disk is not massless.

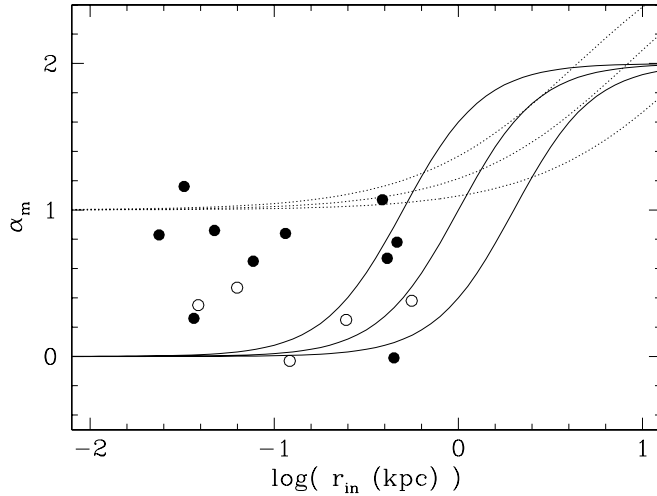


FIG. 12.— Measured inner slope  $\alpha_m$  versus the radius of the innermost point in the rotation curve. The solid lines are the inner slopes of pseudo-isothermal halos with core radii, from left to right, of  $r_c = 0.5, 1, 2$  kpc. The dotted lines are the inner slopes for NFW halos with, from left to right,  $c = 18$  and  $v_{200} = 60$  km s $^{-1}$ ,  $c = 12$  and  $v_{200} = 75$  km s $^{-1}$ , and  $c = 6$  and  $v_{200} = 90$  km s $^{-1}$ . The filled circles represent non-barred galaxies, the open circles represent barred galaxies.

Of course, stellar disks do have mass, and the more dynamically significant they are, the shallower the inner slopes of the dark halos would have to be. In this light, it is interesting to note that the steepest inner slopes are measured in the galaxies with the highest surface brightnesses and presumably the most massive disks (UGC 5721 and UGC 8490), suggesting that for these galaxies the contributions of the stellar disks may have resulted in steeper measured inner slope. On the other hand, we also found galaxies with steep inner slopes among galaxies with low surface brightnesses (e.g., UGC 2259 and F568-V1). These galaxies are dominated by dark matter for stellar mass-to-light ratios of up to a few, and hence the measured inner slopes likely reflect the inner slopes of the dark halos.

The inner slope as derived from the mass density profile has as advantage that it is a parameter free measurement and that it directly measures the inner slope of the halo. However, because it is usually measured from only the innermost points, it is especially sensitive to systematic effects. Also,  $\alpha_m$  generally has a large error, as it is derived from a density profile that depends on the derivative of the observed rotation curve. Because of these uncertainties and systematic effects that may have affected the data, our conclusion is that inner slopes in the range  $0 < \alpha < 1$  are consistent with the observations presented here.

A point of concern raised by dBMBR is that the steep inner slopes do not represent the slopes of the inner parts of the dark matter profiles, but rather the  $r^{-2}$  outer parts. If this were the case, one would expect to see shallow slopes in the best resolved galaxies, and the steepest slopes in the galaxies that are the least well-resolved. To verify this, we used the same test as dBMBR and plotted  $\alpha_m$  against the radius of the innermost point on the rotation curve in Fig. 12. Also drawn are the inner slopes as a function of radius for different pseudo-isothermal halos and NFW halos. From Fig. 12 it is clear that we do find steep inner slopes among the best resolved galaxies, and that the steep slopes of the galaxies in our sample are not the result of the inclusion of the  $r^{-2}$  outer parts.

### 8.1.2. Inner slopes from the mass modeling

Our model observations presented in Section 7.2 have shown that the parameters derived from the mass modeling are less sensitive to the effects of seeing, slit width and slit offsets, because the entire rotation curve is used to determine the parameters, and not only the innermost part. As a consequence, the mass modeling is also less sensitive to the particular value of the inner slope of the dark matter halo (the cusp-core degeneracy), and for most galaxies we find that mass models based on  $\alpha = 1$  provide fits of similar quality as those based on  $\alpha = 0$ . This is not only true if the contribution of the stellar disk is ignored, but also for models in which the stellar disks play a modest role.

Nonetheless, in about 25% of the galaxies the mass models with  $\alpha = 1$  give significantly poorer fits than those based on  $\alpha = 0$ , even if the baryonic component is ignored (UGC 4325, UGC 4499, F563-V2 and F568-3). Even though our modeling in Section 7.2 has shown that the  $\chi^2$  value may be biased by slit offsets, unrealistically large offsets would be required to make the observed rotation curves consistent with a halo with  $\alpha = 1$ . Hence, it is not likely that the poor fits for these four galaxies are the result of alignment errors, except perhaps in the case of UGC 4325, in which the optical center and the dynamical center derived by S99 are offset by 5''.

A possibility is that some of these poor fits are the result of non-circular motions. It is difficult to get an estimate of the strength of non-circular motion from the observations presented here, as our long-slit observations only provide a one-dimensional slice through the velocity field. On the other hand, the optical morphology may provide an indication of whether non-circular motions play a role. As a first order indicator of the presence of non-circular motions, we used the presence of a bar. The galaxies in our sample with either mild or strong bars are UGC 731, UGC 4499, UGC 11861, F563-V2, and F568-3. Interestingly, 3 out of the 4 galaxies which are poorly fit by an NFW halo have strong bars (UGC 4499, F563-V2 and F568-3), suggesting that the non-circular motions associated with bars may have contributed to the poor fits.

In conclusion, we find that almost all galaxies in our sample are consistent with pseudo-isothermal halos. About three quarters of our sample is also consistent with NFW halos, and the remaining quarter may have been affected by non-circular motions. Based on the sample of galaxies presented here, and given the uncertainties, we find that slopes in the range  $0 \lesssim \alpha \lesssim 1$  are consistent with the observations.

## 8.2. Comparison to the literature

Our conclusion that the inner slopes of the dark halos seem consistent both with  $\alpha = 0$  and  $\alpha = 1$  appears to be add odds with the conclusions from dBMBR and dBB, who found that the derived inner slopes for the galaxies in their sample peaks at  $\alpha_m = 0.2$ , with a tail toward steeper slopes.

Here we investigate whether the systematic effects studied in this paper may have played a role in their work. To this end, we have divided the galaxies from the dBMBR and dBB sample in three categories, based on a visual inspection of their optical images: edge-on galaxies, barred galaxies, and the remaining galaxies. We have separated the galaxies into two distance groups, one with galaxies that are closer than 2000 km s $^{-1}$ , and one with galaxies that are more distant than that. As before, the separation in these two distance groups was done to match

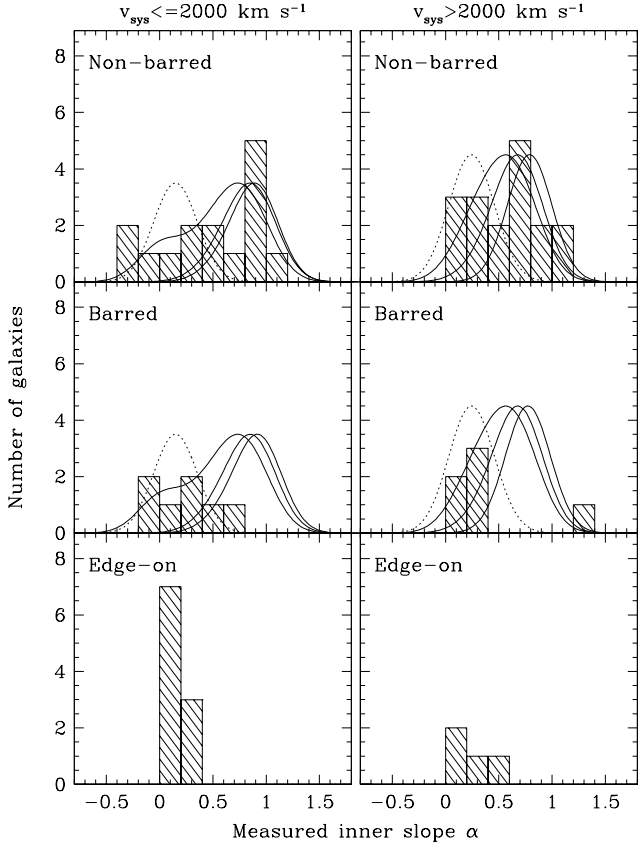


FIG. 13.— The distribution of measured inner slopes for the galaxies in the samples of de Blok et al. (2001a), de Blok & Bosma (2002), and the sample presented here, divided into three groups, both for galaxies within  $2000 \text{ km s}^{-1}$  (left column), and for galaxies beyond  $2000 \text{ km s}^{-1}$ . The shaded histograms in the top panels show the distribution of slopes for non-barred galaxies, the ones in the middle panels for galaxies that are barred, and the ones in the bottom panels for edge-on galaxies. The dotted lines represent the expected distributions of the inner slopes for  $\alpha = 0$ , the solid lines from left to right give the expected distributions for  $\alpha = 1$ , with a slit alignment  $\sigma_{\text{off}}$  of  $2''$ ,  $1''$ , and  $0''$ . A measurement error on  $\alpha_m$  of 0.25 was assumed.

the separation in these two distance groups was done to match the distances used in the models presented in Section 7. We have excluded the three LSB galaxies that dBMBR took from the Verheijen (1997) sample, because these were based on low-resolution HI observations.

We present the distributions of measured inner slopes for each of the categories in Fig. 13. The galaxies in the sample discussed in this paper are also included. For galaxies that are present in both our and the literature studies, we have used the results presented here. Using the modeling results from Section 6, we calculated the expected distribution of observed inner slopes for the non-edge-on and non-barred galaxies, given an intrinsic inner slope of the dark matter distribution, a slit with of  $1.5''$  (the average of the observations in the different samples) and different values for the slit alignment error, for galaxies within  $2000 \text{ km s}^{-1}$ , and for galaxies beyond  $2000 \text{ km s}^{-1}$ . The expected distributions have been calculated in the same way as described in Section 8.1, and are overplotted on the histograms in Fig. 13.

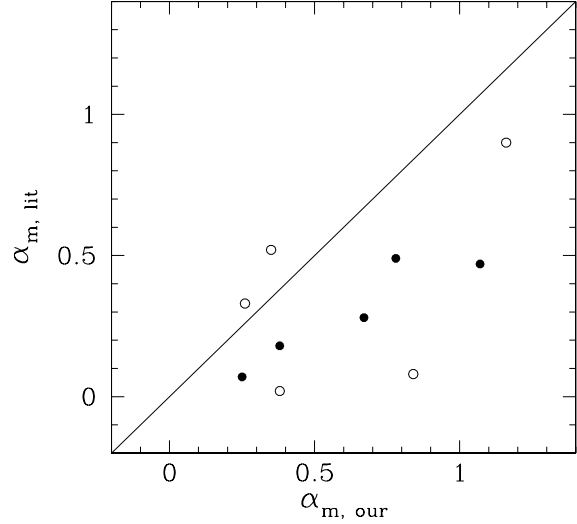


FIG. 14.— Comparison of the values of the inner slopes as derived from density profiles presented in this paper to those in the literature. The filled circles represent galaxies for which the same data was used both here and de Blok et al. (2001a), the open circles represent galaxies for which independent observations were used.

For the non-barred galaxies with  $v_{\text{sys}} < 2000 \text{ km s}^{-1}$ , the measured inner slopes span a wide range from  $\alpha = 0$  to  $\alpha = 1$ , and for the closeby galaxies some galaxies even appear to have negative  $\alpha$ , i.e., a dark matter density that increases with radius. The distribution of  $\alpha_m$  for the non-barred galaxies in the combined sample appears inconsistent with the distribution expected for halos with  $\alpha = 0$ , because of the excess of galaxies with steeper inner slopes. However, it is possible that the stellar disks do contribute significantly and this may explain the wing to high  $\alpha_m$  even if the halos have  $\alpha = 0$ . The models with  $\alpha = 1$  appear to underpredict the number of galaxies with  $\alpha_m$  near zero, unless the error in the slit positioning is about  $2''$ , for which the model is good agreement with the observed distribution. An error of  $2''$  in the slit positioning may not be unreasonable given the large angular size of these galaxies and their irregular, diffuse and low surface brightness nature, and the fact that pointing errors, errors in their optical centers, and possible offsets between optical and dynamical center all contribute.

For the galaxies at 60 Mpc the expected distributions for the different intrinsic halo shapes are more similar, although again it appears as if the model for  $\alpha = 0$  appears to underpredict the number of galaxies with steep slopes.

As before, we have used the presence of a bar as an indicator of the presence of non-circular motions. The distribution of  $\alpha_m$  for the barred galaxies is shown separately in Fig. 13. Although based on only a few galaxies, the barred galaxies on average appear to have a somewhat lower  $\alpha_m$ . This may be an indication that the non-circular motions associated with the bar have affected the inner slopes. On the other hand, if these bars were randomly oriented, one would expect that such non-circular motions would mostly lead to an increased scatter in the rotation curves, as observed by e.g., Sofue et al. (1999), and hence on  $\alpha_m$ , but hardly to systematically lower values. However, in most of the galaxies in both our sample and the literature sample, the bars are not randomly oriented, but preferentially aligned with the major axis in almost all galaxies. This might explain the observed shallower gradients in these

galaxies. Alternatively, the barred galaxies in our sample may have halos with intrinsically shallow inner slopes.

A striking feature in Fig. 13 is the large difference in the distribution of measured inner slopes between edge-on galaxies and the non-barred galaxies, in both distance groups. Although perhaps a result of the possibility that galaxies selected to have low surface brightnesses when seen edge-on have different intrinsic properties than those selected to have low surface brightnesses when seen face-on, a more likely explanation is that this marked difference is artificial. As demonstrated in Section 7.3, the method used here and in several literature studies is not suited to derive rotation curves for edge-on galaxies, as it results in a severe underestimate of the inner slope. In fact, as shown in Section 7.3, this method, when applied to edge-on galaxies dominated by NFW halos, yields an inner slope of  $\alpha_m \sim 0.2$ , close to the peak dBMBR found.

The sample presented in this paper has a number of galaxies in common with the samples presented in dBMR and dB. In Fig. 14 we plot the inner slopes as derived in the literature version those derived there. The filled circles represent the inner slopes derived for the five LSB galaxies presented in SMT. For these five galaxies *the same* data have been analyzed in different ways by dBMR and by us. The open circles represent galaxies for which dB and we have independent observations. As is clear from Fig. 14, the inner slopes derived in this paper generally are steeper than those derived in the literature. The reasons for this difference are not clear. Probably the choice of the break radius within which the inner slope is measured, the fact that dBMR and dB have derived their rotation curves by fitting smooth curves to their data, and the fact that the data have been binned in 2" intervals here and in dBMBR, but 6" for some galaxies in dB all play a role. Irrespective of the cause for the difference, it is clear that when different observers find such different results for the same galaxies, even when the same data are used, the data do not allow firm conclusions to be drawn.

In addition, we compared the derived values for  $c$  and  $v_{200}$  for the galaxies that we have in common with dBMR and dB. In contrast with the results for the derived inner slopes, the derived halo parameters show little or no systematic difference between our and their best fit values, although there is a considerable scatter of about 35% between the best fit values for  $c$ . The fact that there is a systematic difference between the derived inner slopes but hardly in the derived halo parameters is not unexpected. The inner slope is determined solely from the inner few points. On the other hand, the mass modeling uses the entire rotation curve, and the outer parts of the rotation curves both in our and in the literature samples are similar in shape because they both use the HI data from S99.

We have also compared our fitting results to those obtained by Marchesini et al. (2002), who have three galaxies in common with the our sample (UGC 4325, UGC 4499, and UGC 11861). The fits presented in their Fig. 5 strongly overpredict the inner rise of the rotation curves for their NFW models. However, as Marchesini et al. (2002) warn, they did not fit the observed rotation curves, but only normalized each curve to its last point. When instead they make fits using the same mass models as described in Section 4, they find best fit values for  $c$  and  $v_{200}$  in good agreement with our results.

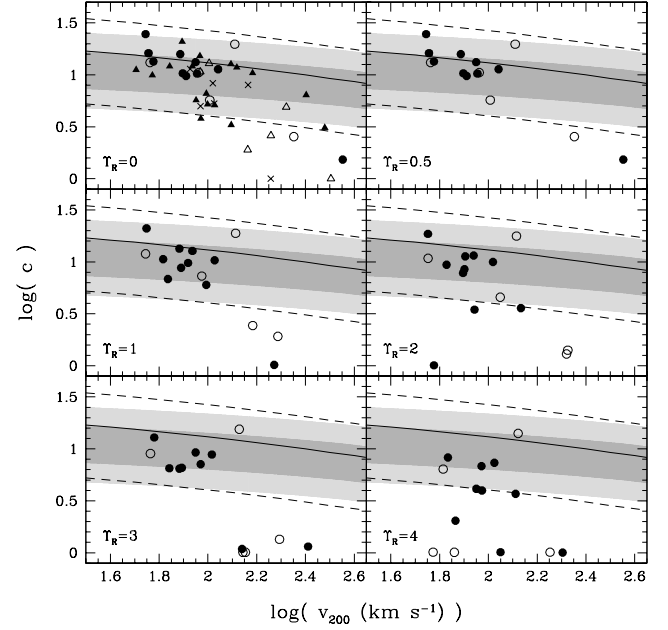


FIG. 15.— The NFW halo concentration  $c$  plotted against the halo rotation velocity  $v_{200}$  for  $\Upsilon_*$  of 0 to 4, as indicated in the lower left corner of each panel. The filled circles represent the non-barred galaxies in our sample, the open circles represent the barred galaxies in our sample. The filled triangles are the non-barred galaxies in the combined samples of de Blok et al. (2001b) and de Blok & Bosma (2002), the open triangles are the barred galaxies, and the crosses the edge-on galaxies. The dark and light shaded regions represent the  $1\sigma$  and  $2\sigma$  limits on the distribution of halo parameters as predicted by Navarro et al. (1997), and the solid and dashed lines represent the mean and  $2\sigma$  limits from the Bullock et al. (2001) model.

### 8.3. The nature of dark matter

The properties of dark matter halos depend on the nature of dark matter and the cosmological parameters. Here we compare the predictions made from simulations based on the currently popular  $\Lambda$ CDM paradigm. There is disagreement between the different cosmological simulations as to what the expected inner slope of the dark matter halos in a universe dominated by CDM is. As noted in the introduction, several studies have reported an inner slope with  $\alpha = 1.5$ , but the most recent simulations seem to prefer  $\alpha \sim 1$ . This difference is crucial, as none of the galaxies in our sample or the literature sample are consistent with  $\alpha = 1.5$ , whereas most of them, given the involved uncertainties, seem consistent with  $\alpha = 1$ . At the same time, none of these galaxies *require* halos with  $\alpha = 1$ , as their rotation curves are usually equally well or better explained by halos with shallower density profiles or even constant density cores.

In Fig. 15 we compare the best-fit values of  $c$  and  $v_{200}$  obtained from fitting mass models to the observed rotation curves with the predictions from the numerical simulations of Navarro et al. (1997) and Bullock et al. (2001). The open and filled circles represent the halo parameters found for the barred and the non-barred galaxies in our sample, the open and filled triangles are the barred and the non-barred galaxies in dBMR and dB, and the crosses are the edge-on galaxies in their sample. We have plotted the results for a range in M/L for the galaxies

in our sample. Note that the fitting results are slightly different from the results listed in Table 2, because in the fitting here the contribution of the HI has been taken into account.

Fig. 15 shows that the majority of the galaxies have values for  $c$  and  $v_{200}$  that are consistent with  $\Lambda$ CDM, provided the M/L of the stellar disk is about 2 or smaller. M/Ls in this range are consistent with predictions from stellar population synthesis models. Based on the typical  $B - R$  color of  $0.84 \pm 0.14$  for the galaxies in this sample (de Blok et al. 1995, Swaters & Balcells 2002), M/Ls in the range 0.4 to 1.4 are expected (e.g., Bell & de Jong 2001). It should be noted, however, that these synthesis models do not provide a normalization of the M/L, and changes in the adopted properties of the stellar initial mass function will change the expected M/Ls. If the M/Ls are larger than 2, more and more galaxies become inconsistent with the predictions of  $\Lambda$ CDM. One galaxy from our sample, UGC 11557, as is also apparent from Table 2, has a low  $c$  as derived from the best fit. However, as is clear from Fig. 1, the rotation curve for this galaxy does not extend much beyond the turnover radius, and hence  $c$  is poorly constrained. Even though  $c = 1$  is the best fit for this galaxy, larger values, up to  $c = 4$  are also consistent with the observed rotation curve.

Barred galaxies seem to have somewhat lower values for  $c$ , and, as shown in Figs. 11, 12 and 13 they also tend to have shallower inner slopes. Although this may be due to non-circular motions, it may also indicate that the barred galaxies in our sample have halos with intrinsically shallower inner slopes. Similar results have been found from observations of barred spiral galaxies. The results from Weiner et al. (2001) for NGC 4123 and Binney & Evans (2001) for the Galaxy indicate that the disks in these galaxies are close to maximal, resulting in low density halos with shallow cores. Such shallow cores appear to be in conflict with the predictions by  $\Lambda$ CDM simulations, although one might envision a scenario in which the interaction between a bar and a cuspy dark halo results in the formation of a constant density core (Weinberg & Katz 2002).

## 9. SUMMARY AND CONCLUSIONS

We presented high resolution H $\alpha$  rotation curves for a sample of 15 dwarf and LSB galaxies derived from long-slit observations. From these, we measured the slope of the central mass distribution, both from the mass density distribution implied by the rotation curves, and from fitting mass models to the rotation curves.

To assess the influence of systematic effects on the derived inner slopes, we have modeled the effects of galaxy inclination, slit width, seeing and slit alignment errors on the derived rotation curves. Other systematic effects that are less easily modeled, such as non-circular motions or the detailed spatial

distribution of H $\alpha$  emission, have been discussed but not modeled. Combined, these systematic effects may lead to a systematic bias toward shallower slopes if the intrinsic halo profile has a steep inner slope. If the inner slope is intrinsically shallow, the inner slope is hardly affected, and may even be somewhat overestimated.

Using the data presented in the paper, and recent data for similar galaxies presented in the literature, we find that both the inner slopes as derived from the mass density profiles and from the mass model fitting indicate that most galaxies in our sample are consistent with the range in intrinsic inner slopes  $0 \lesssim \alpha \lesssim 1$ . Inner slopes with  $\alpha > 1$  are ruled out by these observations. The range of intrinsic inner slopes that appear consistent with the observations is rather large, because the inner slopes as derived from the mass density profiles are susceptible to the systematic effects mentioned in this paper, and because the mass modeling is not very sensitive to the inner slopes (the cusp-core degeneracy). We note that about 25% of the galaxies in our sample appear to be inconsistent with NFW halos. These galaxies are predominantly barred, suggesting either the rotation curves for these galaxies may have been affected by the non-circular motions associated with the bars, or perhaps that the halos of these galaxies intrinsically have shallower slopes. The remaining 75% have best-fit values for their halo parameters that are consistent with the values expected in a  $\Lambda$ CDM cosmology, provided that the  $R$ -band stellar mass-to-light ratios are smaller than about 2.

Even though the majority of the galaxies in this sample seem consistent with steep inner slopes, none of the galaxies *require* halos with  $\alpha = 1$ , as most galaxies are equally well or better fit by halos with shallower density profiles or even constant density cores.

Many of the systematic effects discussed in this paper can be avoided if high-resolution, two-dimensional velocity fields are used. Slit offsets will not play a role, the kinematical centers can be determined directly from the data, and non-circular motions can be mapped and modeled. A detailed study of barred dwarf and LSB galaxies may be particularly interesting.

We thank Vera Rubin and Roelof Bottema for providing useful comments on earlier versions of this paper. This research has made use of the NASA/IPAC Extragalactic Database (NED) which is operated by the Jet Propulsion Laboratory, California Institute of Technology, under contract with the National Aeronautics and Space Administration. RS thanks IPAC for its hospitality during his visits which were funded in part by a grant to BFM as part of the NASA Long-Term Space Astrophysics Program.

## REFERENCES

Barnes, J. & White, S. D. M. 1984, MNRAS, 211, 753  
 Barth, A. J., Sarzi, M., Rix, H., Ho, L. C., Filippenko, A. V., & Sargent, W. L. W. 2001, ApJ, 555, 685  
 Begeman, K. G. 1987, PhD thesis, Rijksuniversiteit Groningen  
 Begeman, K. G. 1989, A&A, 223, 47  
 Bell, E. F. & de Jong, R. S. 2001, ApJ, 550, 212  
 Binney, J. J. & Evans, N. W. 2001, MNRAS, 327, L27  
 Blais-Ouellette, S., Carignan, C., Amram, P., & Côté, S. 1999, AJ, 118, 2123  
 Blais-Ouellette, S., Amram, P., & Carignan, C. 2001, AJ, 121, 1952  
 Blumenthal, G. R., Faber, S. M., Flores, R., & Primack, J. R. 1986, ApJ, 301, 27  
 Boriello, A., Salucci, P. 2001, MNRAS, 323, 285  
 Broeils, A.H. 1992a, PhD thesis, Rijksuniversiteit Groningen  
 Broeils, A.H. 1992b, A&A, 256, 19  
 Bullock, J. S., Kolatt, T. S., Sigad, Y., Somerville, R. S., Kravtsov, A. V., Klypin, A. A., Primack, J. R., & Dekel, A. 2001, MNRAS, 321, 559  
 Carignan, C., & Beaulieu, S. 1989, ApJ, 347, 760  
 Carignan, C., Sancisi, R., & van Albada, T. S. 1988, AJ, 95, 37  
 Casertano, S. 1983, MNRAS, 203, 735  
 Colín, P., Avila-Reese, V., & Valenzuela, O. 2000, ApJ, 542, 622  
 Côté, S. 1995, PhD thesis, Australian National University  
 Côté, S., Carignan, C., & Sancisi, R. 1991, AJ, 102, 904  
 Dalcanton, J. J. & Bernstein, R. A. 2000a, ASP Conf. Ser. 197: Dynamics of Galaxies: from the Early Universe to the Present, 161  
 Dalcanton, J. J. & Bernstein, R. A. 2000b, AJ, 120, 203  
 Davé, R., Spergel, D. N., Steinhardt, P. J., & Wandelt, B. D. 2001, ApJ, 547, 574  
 de Blok, W. J. G., Bosma, A. 2002, A&A, 385, 816 (dBB)

de Blok, W. J. G. & McGaugh, S. S. 1997, MNRAS, 290, 533.

de Blok, W. J. G., van der Hulst, J. M., & Bothun, G. D. 1995, MNRAS, 274, 235

de Blok, W. J. G., McGaugh, S. S., & van der Hulst, J. M. 1996, MNRAS, 283, 18

de Blok, W. J. G., McGaugh, S. S., Bosma, A., & Rubin, V. C. 2001, ApJ, 552, L23 (dBMBR)

de Blok, W. J. G., McGaugh, S. S., & Rubin, V. C. 2001, AJ, 122, 2396 (dBMR)

Dubinski, J. & Carlberg, R. G. 1991, ApJ, 378, 496

Flores, R. A., Primack, J. R. 1994, ApJ, 427, L1

Flores, R., Primack, J. R., Blumenthal, G. R., & Faber, S. M. 1993, ApJ, 412, 443

Fukushige, T., & Makino, J. 1997, ApJ, 477, L9

Knebe, A., Devriendt, J., Mahmood, A., & Silk, J. 2002, MNRAS, 329, 813

Klypin, A., Kravtsov, A. V., Bullock, J., & Primack, J. 2001, ApJ, 554, 903

Lake, G., Feinswog, L. 1989, AJ, 98, 166

Lucy, L. B. 1974, AJ, 79, 745

Marchesini, D., D'Onghia, E., Chincarini, G., Firmani, C., Conconi, P., Molinari, E., Zucca, A. 2002, ApJ, 575, 801

McGaugh, S. S., de Blok, W. J. G. 1998, ApJ, 499, 41

McGaugh, S. S. & Bothun, G. D. 1994, AJ, 107, 530

McGaugh, S. S., Rubin, V. C., & de Blok, W. J. G. 2001, AJ, 122, 2381.

Moore, B. 1994, Nature, 370, 629

Moore, B., Governato, F., Quinn, T., Stadel, J., & Lake, G. 1998, ApJ, 499, L5

Moore, B., Quinn, T., Governato, F., Stadel, J., & Lake, G. 1999, MNRAS, 310, 1147

Navarro, J. F. 1998, astro-ph/9807084

Navarro, J. F., Eke, V. R., & Frenk, C. S. 1996, MNRAS, 283, L72

Navarro, J. F., Frenk, C. S., & White, S. D. M. 1996, ApJ, 462, 563

Navarro, J. F., Frenk, C. S., & White, S. D. M. 1997, ApJ, 490, 493

Power et al. 2002, astro-ph/0201544

Puche, D., Carignan, C., & Wainscoat, R. J. 1991, AJ, 101, 447

Sofue, Y., Tutui, Y., Honma, M., Tomita, A., Takamiya, T., Koda, J., & Takeda, Y. 1999, ApJ, 523, 136.

Swaters, R. A. 1999, PhD thesis, Rijksuniversiteit Groningen (S99)

Swaters, R. A. 2001a, in 'Gas and Galaxy Evolution', eds. J.E. Hibbard, M. Rupen, J. H. van Gorkom, ASP Conf. series 240, p. 325

Swaters, R. A. 2001b, in: Galaxy Disks and Disk Galaxies, eds. J.G. Funes S.J., E.M. Corsini, ASP conf. series 230, p. 545

Swaters, R. A., Balcells, M. 2002, A&A, 390, 863

Swaters, R. A., Madore, B. F., & Trehella, M. 2000, ApJ, 531, L107

Swaters, R. A., van Albada, T. S., van der Hulst, J. M., & Sancisi, R. 2002, A&A, 390, 829

Swaters, R. A., Schoenmakers, R. H. M., Sancisi, R., & van Albada, T. S. 1999, MNRAS, 304, 330

van Albada, T. S., Bahcall, J. N., Begeman, K., Sancisi, R. 1985, ApJ, 295, 305

van den Bosch, F. C., Swaters, R. A. 2001, MNRAS, 325, 1017 (vdBS)

van den Bosch, F. C., Robertson, B. E., Dalcanton, J. J., & de Blok, W. J. G. 2000, AJ, 119, 1579

Verheijen, M. A. W. 1997, PhD thesis, Rijksuniversiteit Groningen

Warmels, R. H. 1988, A&AS, 72, 427

Weinberg, M. D., Katz, N. 2001, astro-ph/0110632

Weiner, B. J., Sellwood, J. A., & Williams, T. B. 2001, ApJ, 546, 931

Worthey, G. 1994, ApJS, 95, 107